Non-equilibrium transport in the Anderson model of a biased quantum dot: Scattering Bethe Ansatz phenomenology

Chao, S.-P.; Palacios, G.

Publication date
2010

Document Version
Submitted manuscript

Non-equilibrium Transport in the Anderson model of a biased Quantum Dot: Scattering Bethe Ansatz Phenomenology

Sung-Po Chao[1] and Guillaume Palacios[1,2]

[1]*Center for Materials Theory, Department of Physics and Astronomy, Rutgers University, Piscataway, NJ 08854*
[2]*Instituut voor Theoretische Fysica, Universiteit van Amsterdam, Valckenierstraat 65, 1018 XE Amsterdam, The Netherlands*

We derive the transport properties of a quantum dot subject to a source-drain bias voltage at zero temperature and magnetic field. Using the Scattering Bethe Anstaz, a generalization of the traditional Thermodynamic Bethe Ansatz to open systems out of equilibrium, we derive *exact* results for the quantum dot occupation out of equilibrium and, by introducing *phenomenological* spin- and charge-fluctuation distribution functions in the computation of the current, obtain the differential conductance for large $\frac{U}{\Gamma}$. The Hamiltonian to describe the quantum dot system is the Anderson impurity Hamiltonian and the current and dot occupation as a function of voltage are obtained numerically. We also vary the gate voltage and study the transition from the mixed valence to the Kondo regime in the presence of a non-equilibrium current. We conclude with the difficulty we encounter in this model and possible way to solve them without resorting to a *phenomenological* method.

PACS numbers: 72.63.Kv, 72.15.Qm, 72.10.Fk

I. INTRODUCTION

The past few years have witnessed a spectacular progress in the fabrication and exploration of nano-structures giving experimentalists unprecedented control over the microscopic parameters governing the physics of these systems. Nano-structures, beyond their practical applications, display an array of emergent phenomena stemming from their reduced dimensionality which enhances quantum fluctuations and strong correlations. Often, experiments are carried out under non-equilibrium conditions, with currents passing through the structures. The measurements are performed over a wide range of parameters, such as temperature and applied bias, allowing experimental exploration of the interplay between non-equilibrium dynamics and strong correlation physics[1–6]. A canonical example is the non-equilibrium Kondo effect observed in a quantum dot attached to two leads held at different chemical potentials μ_i. The voltage difference $V = \mu_1 - \mu_2$ induces a non-equilibrium current $I(V)$ through the dot, interfering with and eventually destroying the Kondo effect as the voltage is increased.

In this paper we develop a *phenomenological* approach, based on an exact method, the Scattering Bethe Ansatz (SBA), recently developed by P. Mehta and N. Andrei (MA)[7], a non-perturbative implementation of the Keldysh formalism to construct the current-carrying, *open-system* scattering eigenstates for the two-lead nonequilibrium Anderson impurity model, the standard model to describe the system[8–21]. The basic idea of SBA is to construct scattering eigenstate of the full Hamiltonian defined directly on the infinite line and match the incoming states by two fermi seas describing the initial state of the leads. The non-equilibrium steady state transport properties of the system are then expressed as expectation values of the current or dot occupation operators in these eigenstates. This program has been implemented for the Interacting Resonance Level Model (IRLM), a spinless interacting model, described in Ref. 7 where the zero temperature results for current and dot occupation $\langle \hat{n}_d \rangle$ for all bias voltages were presented. Another exact solution of this model at the so-called self-dual point[22] by E. Boulat, H. Saleur and P. Schmitteckert in Refs. 23,24 uses the comformal field theory and compares with t-DMRG results.

Carrying out the program for the non-equilibrium Anderson model we find difficulties in the direct application of the SBA approach due the fact that the ground state in the Bethe basis consists of bound pairs of quasi-particles, leading to problems in the computation of the scattering phase shifts for the quasi-particles with complex momenta. This problem is not present in the IRLM when the Bethe momenta are below the impurity level and no bound states can be formed. We circumvent this difficulty by means of the following arugment: The transport property computed in the IRLM is related to the single particle phase shift across the impurity in the Bethe basis. Based on the same idea we develop a phenomenological approach to describe the transport property in the Anderson impurity model. We identify two types of possible phase shifts across impurity, which we refer to as "spin-fluctuation" and "charge-fluctuation" types to label two phenomenological phase shifts akin to the fundamental excitations described in the traditional Bethe Ansatz in this model. The phenomenological Ansatz is checked against exact results on the dot occupation in equilibrium and the Friedel sum rule[25,26], in the linear response regime. Subsequently, we discuss our results for the out of equilibrium current, conductance and dot occupation. The scaling relations for the conductance, predicted from the Fermi liquid picture of the problem at strong and weak coupling, are also discussed.

The paper is organized as follows. We start with a formal construction of scattering eigenstates in the two-

lead Anderson impurity model. Then we discuss how we impose boundary conditions, which serve as initial condition in the time dependent picture, on the electrons within the leads. Next we shall discuss our results for the dot occupation in equilibrium and the conductance in the linear response regime. Based on the checks in equilibrium we then extend our computation to the out of equilibrium regime. The difficulty we encounter for complex momenta and the way we handle it will also be addressed there. Comparison with another attempt of exact solution for this model by R. M. Konik et al[27,28] with the idea of dressed excitations above Fermi energy in the Bethe Ansatz picture, first considered for the exact conductance of point contact device in the FQHE regime[29,30], will be discussed. We will also comment on the validity and implication of our numerical results, among them the *exact* charge susceptibility, in the out-of-equilibrium regime. Qualitative agreement between our theory and experimental result is then presented. The limit of $U \to \infty$ is also summarized in the last section based on the same phenomenological approach. Finally, we summarize our results and conclude with some issues on the SBA approach to this model, and state how they could be overcome.

II. THE SCATTERING BETHE ANSATZ APPROACH

A. Scattering state construction

In this section we apply the SBA approach to construct the scattering states of the full Hamiltonian. The (unfolded) 2-lead Anderson impurity Hamiltonian reads,

$$\hat{H} = \sum_{i=1,2} \int \mathrm{d}x\, \psi^\dagger_{i\sigma}(x)(-i\partial_x)\psi_{i\sigma}(x) + \epsilon_d d^\dagger_\sigma d_\sigma + t_i(\psi^\dagger_{i\sigma}(0)d_\sigma + d^\dagger_\sigma \psi_{i\sigma}(0)) + U\, d^\dagger_\uparrow d_\uparrow d^\dagger_\downarrow d_\downarrow \quad (1)$$

where summation over the spin indices σ is implied. The fields $\psi_{i\sigma}(x)$ describe chiral, right-moving electrons from lead i, U is the on-site Coulomb repulsion between electrons on the dot, t_i is the coupling between the dot and the lead i, and ϵ_d is the gate voltage. We have set the Fermi velocity $v_F = 1$.

The model's equilibrium properties have been studied in great detail via the traditional Thermodynamic Bethe Ansatz (TBA)[31,32]. The SBA exploits in a new way the integrability of the Anderson Model to construct current-carrying scattering eigenstates on the open line. There are two main requirements: One is the construction of scattering eigenstates with the number of electrons in each lead conserved prior to scattering off the impurity. Another is the asymptotic boundary condition: that the wave function of the incoming electrons, i.e. in the region ($x \ll 0$), tend to that of two free Fermi seas far from the impurity[7]. All information about the external bias applied to the system is encoded in the boundary condition by appropriately choosing the chemical potential of the incoming Fermi seas. As in all Bethe-Ansatz constructions, the full multi-particle wavefunction is constructed from single particle eigenstates (now on the infinite open line) and the appropriate two-particle S-matrices. We first rewrite Eq. (1) in the even-odd basis as

$$\begin{aligned}
\hat{H} &= \hat{H}_e + \hat{H}_o \\
\hat{H}_e &= \sum_\sigma \int \mathrm{d}x\, \psi^\dagger_{e\sigma}(x)(-i\partial_x)\psi_{e\sigma}(x) + \epsilon_d d^\dagger_\sigma d_\sigma \\
&\quad + t(\psi^\dagger_{e\sigma}(0)d_\sigma + d^\dagger_\sigma \psi_{e\sigma}(0)) + U d^\dagger_\uparrow d_\uparrow d^\dagger_\downarrow d_\downarrow \\
\hat{H}_o &= \sum_\sigma \int \mathrm{d}x\, \psi^\dagger_{o\sigma}(x)(-i\partial_x)\psi_{o\sigma}(x)
\end{aligned}$$

With

$$\begin{aligned}
\psi_{e\sigma}(x) &= \frac{t_1\psi_{1\sigma}(x) + t_2\psi_{2\sigma}(x)}{\sqrt{t_1^2+t_2^2}} \\
\psi_{o\sigma}(x) &= \frac{t_2\psi_{1\sigma}(x) - t_1\psi_{2\sigma}(x)}{\sqrt{t_1^2+t_2^2}}
\end{aligned}$$

and $t = \sqrt{t_1^2+t_2^2}$. In what follows we consider the case $t_1 = t_2 = \frac{t}{\sqrt{2}}$ for simplicity. The single particle solution for even and odd basis is: $|e, p\sigma\rangle = \int \mathrm{d}x\, (e^{ipx} g_p(x)\psi^\dagger_{e\sigma}(x) + e_p\delta(x)d^\dagger_\sigma)|0\rangle$ and $|o, p\sigma\rangle = \int \mathrm{d}x\, e^{ipx} h_p(x)\psi^\dagger_{o\sigma}(x)|0\rangle$, with $|0\rangle$ the vacuum state and $g_p(x)$, $h_p(x)$, e_p independent of spin and given by

$$\begin{aligned}
&g_p(x) = \theta(-x) + e^{i\delta_p}\theta(x) + s_{ep}\,\theta(x)\theta(-x)\ , \\
&h_p(x) = \theta(-x) + \theta(x) + s_{op}\,\theta(x)\theta(-x)\ , \\
&e_p = \frac{t(1 + e^{i\delta_p} + s_{ep}/2)}{2(p-\epsilon_d)}\ .
\end{aligned} \quad (2)$$

Here $\delta_p \equiv 2\tan^{-1}(\frac{\Gamma}{\epsilon_d - p})$ is the single particle scattering phase shift of the electrons off the impurity with $\Gamma \equiv \frac{t^2}{2}$ being the width of the resonance level. We adopted a symmetric regularization scheme $\theta(\pm x)\delta(x) = \frac{1}{2}\delta(x)$ and imposed $|p| \le D$, D being the bandwidth cut-off[34]. The $s(x) = \theta(x)\theta(-x)$ term is a local constant ($\partial_x s(x) = 0$) in this scheme and it is included in the odd channel function to allow the same two particle S-matrices, Eq.(4), in all channels[35]. The $\theta(x)\theta(-x)$ term in the even channel wave function is introduced in order to modify the single particle phase shift across the impurity. The choice of s_{op} and s_{ep} will be addressed later. In the lead basis, $|i, p\sigma\rangle$, the single-particle scattering eigenstates with the incoming particle incident from lead i, can be restored by taking a proper linear combination of even-odd states. For example, $|1, p\sigma\rangle = \frac{1}{\sqrt{2}}(|e, p\sigma\rangle + |o, p\sigma\rangle)$ is written as

$$|1, p\sigma\rangle = \int \mathrm{d}x\, e^{ipx}\Big\{[\theta(-x) + \frac{1}{2}(e^{i\delta_p}+1)\theta(x)]\psi^\dagger_{1\sigma}(x) + \frac{1}{2}(e^{i\delta_p}-1)\theta(x)\psi^\dagger_{2\sigma}(x) + e_p d^\dagger_\sigma \delta(x) + s^\dagger_{1p\sigma}(x)\Big\}|0\rangle \quad (3)$$

with $|2,p\sigma\rangle = \frac{1}{\sqrt{2}}(|e,p\sigma\rangle - |o,p\sigma\rangle)$ and $s^\dagger_{ip\sigma}(x)$ related to the $\theta(x)\theta(-x)$ terms. These states have a single incoming particle ($x<0$) from lead i, that is reflected back into lead i with amplitude, $R_p = (e^{i\delta_p}+1)/2$ and transmitted to the opposite lead with amplitude $T_p = (e^{i\delta_p}-1)/2$. Similar single particle states are discussed in Ref. 7.

The multi-particle Bethe-Ansatz wave-function is constructed by means of the two-particle S-matrix, $\mathbf{S}(p,k)$, describing the scattering of two electrons with momenta p and k. The two-particles solution in spin singlet state takes the following form

$$|ik,\uparrow;jp,\downarrow\rangle = \int dx_1 dx_2 A\{e^{i(kx_1+px_2)}Z_{kp}(x_1-x_2)\alpha^\dagger_{ik,\uparrow}(x_1)\alpha^\dagger_{jp,\downarrow}(x_2)\}|0\rangle$$

Here $\int dx e^{ik_i x}\alpha^\dagger_{ik_i,a_i}(x_i) = |ik_i,a_i\rangle$ with a multiplication factor $\tilde{Z}_{kp}(0) \equiv \frac{k+p-2\epsilon_d}{k+p-U-2\epsilon_d}Z_{kp}(0)$ multiplied on the $d^\dagger_\uparrow d^\dagger_\downarrow$ term in two particles eigenstate. The explicit form for this two particles case is written in Eq. (C5). In general we denote the $Z^{a_i,a_j}_{k_i,k_j}(x_i-x_j)$ as $\mathbf{S}^{a_i a_i^{'}}_{a_j a_j^{'}}(k_i,k_j)$ with a_i denotes the spin index before the scattering and $a_i^{'}$ the spin index after the scattering. The matrices must satisfy the Yang-Baxter equations

$$\begin{aligned}&\mathbf{S}^{a_1 a_1^{'}}_{a_2 a_2^{'}}(k_1,k_2)\mathbf{S}^{a_1 a_1^{'}}_{a_3 a_3^{'}}(k_1,k_3)\mathbf{S}^{a_2 a_2^{'}}_{a_3 a_3^{'}}(k_2,k_3)\\ &= \mathbf{S}^{a_2 a_2^{'}}_{a_3 a_3^{'}}(k_2,k_3)\mathbf{S}^{a_1 a_1^{'}}_{a_3 a_3^{'}}(k_1,k_3)\mathbf{S}^{a_1 a_1^{'}}_{a_2 a_2^{'}}(k_1,k_2)\end{aligned}$$

for such a construction to be consistent.

By choosing $s_{op} = -4$ in Eq. (3) (the choice of s_{ep} will be discussed in section B and does not affect the result here) in the single particle states we can construct the same two-particles S-matrix for all combinations in even-odd basis with the two-particles S-matrix (see Appendix. B) given by

$$\mathbf{S}_{\tau,\tau'}(k,p) = \frac{(B(k)-B(p))\mathbf{I}_{\tau,\tau'} + i2U\Gamma\,\mathbf{P}_{\tau,\tau'}}{B(k)-B(p)+i2U\Gamma} \qquad (4)$$

with $B(k) = k(k-2\epsilon_d-U)$, $\mathbf{P}_{\tau,\tau'} = \frac{1}{2}(1+\vec{\sigma}_\tau\cdot\vec{\sigma}_{\tau'})$ the spin exchange operator. Since the S-matrix is the same for all even-odd combinations the S-matrix does not depend on the lead index i, and the number of electrons in a lead, N_i, can change only at the impurity site. This circumstance allows us to construct the fully-interacting eigenstates of our Hamiltonian characterized by the incoming quantum numbers, N_1 and N_2 the numbers of incident electrons from lead 1 and 2 respectively. These quantum numbers are subsequently determined by the chemical potentials μ_1 and μ_2.

To complete the construction of the SBA current-carrying, scattering eigenstate, $|\Psi,\mu_i\rangle$, we must still choose the "Bethe-Ansatz momenta" $\{p_l\}_{l=1}^{N_1+N_2}$ of the single particles states to ensure that the incoming particles look like two Fermi seas in the region $x<0$. This requirement translates into a set of "free-field" SBA equations for the Bethe-Ansatz momenta-density of the particles from the two leads[7]. The argument is as follows: Away from the impurity $|i,p\sigma\rangle$ reduces to $\psi^\dagger_{i\sigma}(x)$ with the inter-particle S-matrix Eq. (4) present. Thus the scattering eigenstates describing non-interacting electrons are in the Bethe basis rather than in the Fock basis of plane waves. The existence of many bases for the free electron is due to their linear spectrum which leads to degeneracy of the energy eigenvalues. The wave function $e^{ip_1x_1+ip_2x_2}[\theta(x_1-x_2) + \mathbf{S}\theta(x_2-x_1)]A$ is an eigenstate of the *free* Hamiltonian for any choice of $\mathbf{S}$ with, in particular, $\mathbf{S} = \mathbb{1}$ defining the Fock basis and $\mathbf{S}$ given in Eq. (4) defining the Bethe basis. The Bethe basis is the correct "zero order" choice of a basis in the degenerate energy space required in order to turn on the interactions. We proceed to describe the leads (two free Fermi seas) in this basis.

We consider the system at zero temperature and zero magnetic field in this paper. To describe the two Fermi seas on the leads translates to a set of Bethe Ansatz equations whose solution in this case consists of complex conjugate pairs: $p^\pm(\lambda) = x(\lambda) \mp iy(\lambda)$ in the λ-parametrization[31–33] with

$$\begin{aligned}x(\lambda) &= \tilde{\epsilon}_d - \sqrt{\frac{\lambda+\tilde{\epsilon}_d^2+\sqrt{(\lambda+\tilde{\epsilon}_d^2)^2+U^2\Gamma^2}}{2}}\\ y(\lambda) &= \sqrt{\frac{-(\lambda+\tilde{\epsilon}_d^2)+\sqrt{(\lambda+\tilde{\epsilon}_d^2)^2+U^2\Gamma^2}}{2}}.\end{aligned}$$

with $\tilde{\epsilon}_d = \epsilon_d + U/2$. Each member of a pair can be either in lead 1 or in lead 2, since the S-matrix is unity in the lead space. There are, therefore, two possible configurations for these bounded pairs. One possible way of forming bounded pairs is described by four types of complex solutions whose densities we denote $\sigma_{ij}(\lambda)$ with $\{ij\} = \{11,12,21,22\}$ indicating the incoming electrons from lead i and lead j. The other possibility, which is perhaps more intuitive in comparing with the free electron in the Fock basis, is to include only $\{ij\} = \{11,22\}$. These two types of states give the same results when evaluating the expectation value of the dot occupation in equilibrium. However when we turn on the bias voltage, the results obtained from a 4-bound states description show some charge fluctuations even way below the impurity level which is not expected from the non-interacting ($U\to 0$) theory (shown in Appendix A). Thus we shall focus on the 2-bound states description in the following discussion.

To describe in the Bethe basis the two leads as two Fermi seas filled up to μ_1 and μ_2, respectively, these densities must satisfy the SBA equations,

$$\begin{aligned}2\sigma_i(\lambda) = -\frac{1}{\pi}\frac{\mathrm{d}x(\lambda)}{\mathrm{d}\lambda}\theta(\lambda-B_i)\\ - \sum_{j=1,2}\int_{B_j}^{\infty}\mathrm{d}\lambda'\; K(\lambda-\lambda')\sigma_j(\lambda')\end{aligned} \qquad (5)$$

with $K(\lambda) = \frac{1}{\pi}\frac{2U\Gamma}{(2U\Gamma)^2+\lambda^2}$. Each density is defined on a domain extending from B_i to the cutoff D - to be sent to infinity. The B_i play the role of chemical potentials for the Bethe-Ansatz momenta and are determined from the physical chemical potentials of the two leads, μ_i, by minimizing the *charge free energy*,

$$F = \sum_i (E_i - \mu_i N_i) = 2\sum_i \int_{B_i}^{\infty} \mathrm{d}\lambda\,(x(\lambda) - \mu_i)\sigma_i(\lambda) \quad (6)$$

with σ_1 the lead 1 particle density and σ_2 the lead 2 particle density. Note that σ_1 and σ_2 obeys the same integral equation Eq. (5) with different boundary ($\sigma_1(\lambda)$ with $\lambda \subset (B_1, \infty)$ and $\sigma_2(\lambda)$ with $\lambda \subset (B_2, \infty)$). Solving the SBA equations subject to the minimization of the charge free energy fully determines the current-carrying eigenstate, $|\Psi, \mu_i\rangle$ and allows for calculation of physical quantities by evaluating expectation value of the corresponding operators. In the following we shall discuss our results from equilibrium cases to non-equilibrium ones, starting with the expression for various expectation value of physical quantities.

B. Expectation value of current and dot occupation

For $\mu_1 = \mu_2$ all B_i are equal to some equilibrium boundary B fixed by the choice of μ_i. The dot occupation is given by the expectation value $\sum_\sigma \langle \Psi, \mu_i | d_\sigma^\dagger d_\sigma | \Psi, \mu_i \rangle$. Taking the limit $L \to \infty$ (L being the size of the lead) one can express n_d as an integral over the density of λ and some matrix element $\nu(\lambda) \simeq \frac{\langle p^+(\lambda)p^-(\lambda)| \sum_\sigma d_\sigma^\dagger d_\sigma |p^+(\lambda)p^-(\lambda)\rangle}{\langle p^+(\lambda)p^-(\lambda)|p^+(\lambda)p^-(\lambda)\rangle}$ taken to order $\frac{1}{L}$. Here we address the different choice of s_{ep} (with $s_{op} = -4$ fixed to have the same S-matrix in all channels) which gives rise to different forms of $\nu(\lambda)$. We shall first discuss $s_{ep} = 0$ and show it reproduces the *exact* result for the dot occupation in equilibrium. While in checking the condition for out-of-equilibrium it fails. Thus we propose $s_{ep} \neq 0$ schemes to circumvent this difficulty and check our proposed scheme against the *exact* equilibrium answer in the second part of the discussion.

(1) $s_{ep} = 0$: We choose $s_{ep} = 0$ as in the case of the 1-lead Anderson impurity model. Denote $\nu(\lambda) = \nu^{SBA}(\lambda)$ in this choice. The dot occupation expectation value in equilibrium is given by

$$n_d = \frac{\langle \Psi, \mu_1 = \mu_2 | \sum_\sigma \hat{d}_\sigma^\dagger \hat{d}_\sigma | \Psi, \mu_1 = \mu_2 \rangle}{\langle \Psi, \mu_1 = \mu_2 | \Psi, \mu_1 = \mu_2 \rangle} = 2\int_B^\infty \mathrm{d}\lambda\,\sigma(\lambda)\nu^{SBA}(\lambda) \quad (7)$$

where the factor 2 in front of the integral accounts for the spin degeneracy. The matrix element of the operator $d_\sigma^\dagger d_\sigma$ in the SBA state is given by

$$\nu^{SBA}(\lambda) = \frac{2\Gamma}{\tilde{x}^2(\lambda) + \tilde{y}_+^2(\lambda)} + \frac{16y(\lambda)\Gamma^2}{[\tilde{x}^2(\lambda) + \tilde{y}_-^2(\lambda)][\tilde{x}^2(\lambda) + \tilde{y}_+^2(\lambda)]} \left(\frac{\tilde{x}(\lambda)}{2\tilde{x}(\lambda) - U}\right)^2 .$$

where we introduced, for simplified notations, the functions $\tilde{x}(\lambda) = x(\lambda) - \epsilon_d$ and $\tilde{y}_\pm(\lambda) = y(\lambda) \pm \Gamma$.

Eq. (7) can be proved to be exact by comparing it with the traditional Bethe Ansatz (TBA) result. In the latter, n_d is computed as the integral of the impurity density. This observation that the SBA and TBA results for n_d agree in equilibrium shows the connection between the dot occupation and the dressed phase shift across the impurity. The proof of this equivalence is given in Appendix C.

To describe the out-of-equilibrium state we first check if the steady state condition $\frac{d\langle \hat{n_d} \rangle}{dt} = 0$ (or equivalently, $\frac{d\langle \hat{N_1} + \hat{N_2} \rangle}{dt} = 0$) is satisfied in this basis. As mentioned earlier these scattering states are formed by bounded quasiparticles with complex momenta and therefore the single particle phase across the impurity is not well defined in the sense that $|e^{i\delta_{p^\pm}}| \neq 1$. This problem begins to surface as we set out to evaluate transport expectation value and renders

$$\frac{d\langle \hat{n_d} \rangle}{dt} = \int_{B_{11}}^{B_{22}} d\lambda \sigma_b(\lambda)\Delta(\lambda) \neq 0 \quad (8)$$

with

$$\Delta(\lambda) = \frac{y^2(\lambda)\Gamma^2}{[\tilde{x}^2(\lambda) + \tilde{y}_-^2(\lambda)][\tilde{x}^2(\lambda) + \tilde{y}_+^2(\lambda)]} .$$

Thus it appears that using this basis the steady state condition is not observed. This problem does not appear when the momenta are real as in the IRLM case[7].

(2) $s_{ep} \neq 0$: To remedy this problem we redefine the single particle phase shifts across the impurity, in analogy to the results for the IRLM[7], through the choice of nonzero s_{ep} in Eq.(3). With a suitable choice of s_{ep} we may restore a well defined single particle phase $|e^{i\tilde{\delta}_p^\pm}| = 1$ with $\tilde{\delta}_p^\pm$ denoting this new phase. The way we judge whether we make the correct choice for the new phases $\tilde{\delta}_p^\pm$ is to compare the dot occupation n_d in equilibrium before and after the redefined phase. The explicit form

of s_{ep} and phase $\tilde{\delta}_p^{\pm}$ will be motivated below but first we shall show that a single redefined phase is not sufficient to satisfy the constraint of dot occupation comparison.

Again the choice of new phases is constrained by the requirement that we shall obtain the same result for $\langle\sum_\sigma d_\sigma^\dagger d_\sigma\rangle$ as given by $\nu^{SBA}(\lambda)$ in equilibrium. Based on this constraint it can be shown explicitly that a single well defined phase (in the sense of $|e^{i\tilde{\delta}_p}|=1$) is not sufficient to reproduce the equilibrium $\nu^{SBA}(\lambda)$ as following: The new dot amplitude $\tilde{e}_{p^+}$ and $\tilde{e}_{p^-}$ have to satisfy

$$\begin{aligned} |\tilde{e}_{p^+}|^2+|\tilde{e}_{p^-}|^2 &= \frac{4\Gamma}{\tilde{x}^2(\lambda)+\tilde{y}_+^2(\lambda))}\ , \\ |\tilde{e}_{p^+}|^2|\tilde{e}_{p^-}|^2 &= \frac{4\Gamma^2}{[\tilde{x}^2(\lambda)+\tilde{y}_+^2(\lambda)][\tilde{x}^2(\lambda)+\tilde{y}_-^2(\lambda)]}\ . \end{aligned}$$

As both $|\tilde{e}_{p^+}|^2$ and $|\tilde{e}_{p^-}|^2$ are positive we see that a single redefined phase cannot satisfy the above constraints simultaneously. Therefore we have to choose at least two sets of redefined phases $\tilde{\delta}^i_{p^\pm}$ (with $i=s,h$ denoting spin-fluctuation or charge-fluctuation to be addressed later) and, along with them, some distribution functions f^i to set the weight for these phases.

To motivate the idea of searching the correct phase shifts we shall come back to the derivation of dot occupation in traditional Bethe Ansatz (TBA) picture. In TBA the total energy of the system is described by energy of the leads electrons and energy shifts from the impurity,

$$E=\sum_j p_j=\sum_j\left(\frac{2\pi n_j}{L}+\frac{1}{L}\delta_j\right) \tag{9}$$

Based on Feynman-Hellman theorem, which is applicable in equilibrium (closed) system, we have

$$\langle\hat{n}_d\rangle=\frac{\partial E}{\partial\epsilon_d}=\frac{1}{L}\sum_j\frac{\partial\delta_j}{\partial\epsilon_d}=\frac{1}{L}\sum_j\frac{\partial(\delta_{p_j^+}+\delta_{p_j^-})}{\partial\epsilon_d} \tag{10}$$

The result for Eq. (10) agrees with those obtained from Eq. (C2) and can be viewed as a third approach to obtain the expectation value of the dot occupation. The key observation here is that this quantity is related to the *bare* phase shift $\delta_{p^+}+\delta_{p^-}$ and therefore the redefined phases must be proportional to this quantity. Among them there are two likely candidates with redefined phase shift given by $\delta_{p^+}+\delta_{p^-}$, describing the tunneling of a bounded pair, and $\frac{\delta_{p^+}+\delta_{p^-}}{2}$, describing the tunneling of a single quasi-particle. In a sense this is the echo for the elementary excitations above the Fermi surface in the Bethe basis characterized by N. Kawakami and A. Okiji[36] as charge-fluctuation excitation, which describes bounded pair quasi-particles excitation, and spin-fluctuation excitation, which describes one quasi-particle excitation. Another similar picture is the spin-fluctuation and charge-fluctuation two fluids picture proposed by D. Lee et al[37] albeit in a different context. We identify the phase defined by

$$\tilde{\delta}_{p^-}=\tilde{\delta}_{p^+}=\frac{\delta_{p^+}+\delta_{p^-}}{2}\equiv\tilde{\delta}_p^s$$

(with $s_{ep^\pm}\equiv s^s_{ep^\pm}=\frac{2}{\Gamma}(i(p^\pm-\epsilon_d)-\Gamma)(e^{i(\frac{\delta_{p^+}+\delta_{p^-}}{2})}-1)$) as spin-fluctuation phase shift and

$$\tilde{\delta}_{p^-}=\tilde{\delta}_{p^+}=\delta_{p^+}+\delta_{p^-}\equiv\tilde{\delta}_p^h$$

(with $s_{ep^\pm}\equiv s^h_{ep^\pm}=\frac{2}{\Gamma}(i(p^\pm-\epsilon_d)-\Gamma)(e^{i(\delta_{p^+}+\delta_{p^-})}-1)$) as charge-fluctuation phase shift.

The out-of-equilibrium current is evaluated by the expectation value of current operator $\hat{I}$ with $\langle\hat{I}\rangle$ defined by

$$\langle\hat{I}\rangle=\frac{-\sqrt{2}iet}{\hbar}\langle\sum_\sigma((\psi^\dagger_{1\sigma}(0^\pm)-\psi^\dagger_{2\sigma}(0^\pm))d_\sigma-h.c.)\rangle \tag{11}$$

in the state $|\Psi,\mu_i\rangle$. Notice that $\psi^\dagger_{i\sigma}(0^\pm)\equiv\lim_{\epsilon\to0}(\psi^\dagger_{i\sigma}(-\epsilon)+\psi^\dagger_{i\sigma}(+\epsilon))/2$ is introduced in transport related quantity to be consistent with our regularization scheme which introduces another local discontinuity in odd channel at impurity site.

From Eq. (11) and the expression for the phases $\tilde{\delta}^s_p$ and $\tilde{\delta}^h_p$ we have the expression for current as

$$\begin{aligned} I(\mu_1,\mu_2)&=\langle\Psi,\mu_1,\mu_2|\hat{I}|\Psi,\mu_1,\mu_2\rangle \\ &=\frac{2e}{\hbar}\int_{B_1}^{B_2}\mathrm{d}\lambda\ \sigma_b(\lambda)(f_s(\lambda)J^s(\lambda)+f_h(\lambda)J^h(\lambda)) \end{aligned} \tag{12}$$

The corresponding spin-fluctuation and charge-fluctuation matrix element of the current operator, denoted as $J^s(\lambda)$ and $J^h(\lambda)$, are given by

$$J^s(\lambda) = 1+\frac{\mathrm{sgn}(\tilde{x}(\lambda))(\tilde{x}^2(\lambda)+y^2(\lambda)-\Gamma^2)}{\sqrt{(\tilde{x}^2(\lambda)+y^2(\lambda)-\Gamma^2)^2+4\Gamma^2\tilde{x}^2(\lambda)}} \tag{13}$$

$$J^h(\lambda) = \frac{2\Gamma^2\tilde{x}^2(\lambda)}{(\tilde{x}^2(\lambda)+\Gamma^2)^2-2y^2(\lambda)(\Gamma^2-\tilde{x}^2(\lambda))+y^4(\lambda)}. \tag{14}$$

Here $\mathrm{sgn}(x)=\frac{x}{|x|}$ is the sign function. It is introduced in order to pick up the correct branch when taking the square root in denominator of Eq. (13). This way we ensure that $J^s(\lambda)$ has the proper limit when U is sent to infinity (cf Section III). Other than the motivations mentioned above for identifying spin and charge fluctuation phase shifts the functional forms of $J^s(\lambda)$ and $J^h(\lambda)$ as a function of bare energy $x(\lambda)$ can also be used to identify these two type of phase shifts (See Fig. 11 in Section III for infinite U Anderson model, the finite U is similar).

Next we shall choose the appropriate weight for each type of phase shift. So far we have not yet been able to deduce the form of these weight functions $f_s(\lambda)$ and $f_h(\lambda)$ and we introduce them *phenomenologically*. Let us define *phenomenological* spin-fluctuation and charge-fluctuation weight functions as

$$f_s(\varepsilon(\lambda))=\frac{D_s(\varepsilon(\lambda))}{D_s(\varepsilon(\lambda))+D_h(\varepsilon(\lambda))} \tag{15}$$

and

$$f_h(\varepsilon(\lambda)) = \frac{D_h(\varepsilon(\lambda))}{D_s(\varepsilon(\lambda)) + D_h(\varepsilon(\lambda))} \,. \tag{16}$$

Here $D_s(\varepsilon(\lambda))$ is the spin-fluctuation density of state, $D_h(\varepsilon(\lambda))$ is the charge-fluctuation density of state as defined in Ref. 36, and $\varepsilon(\lambda)$ is the corresponding dressed energy i.e. the energy required to produce these spin- and charge-fluctuation excitations above the Fermi level. Here dressed energy refers to the sum of the bare energy of adding/removing one bound state, as in charge fluctuation, or single quasi particle, as in spin fluctuation, and the energy shift from other quasi particles due to this change. The equation that solves a single quasi-particle's dressed energy $\varepsilon(\lambda)$ reads[38]

$$\varepsilon(\lambda) = (x(\lambda) - \mu) - \int_B^\infty \mathrm{d}\lambda' \, K(\lambda - \lambda')\varepsilon(\lambda') \,. \tag{17}$$

We wish to compare at this point our approach to the one taken by Konik et al[27,28]. The authors' Landauer approach is based on an ensemble of renormalized excitations, the holons and spinons, and the conductance is expressed in terms of their phase shift crossing the impurity. However, the leads are built of bare electrons and thus one faces the difficult problem of how to construct a bare electron out of renormalized excitations in order to be able to impose the voltage boundary condition. The basic approximation adopted, *electron* $\approx$ *antiholon + spinon*, is valid only when the electron is close to the Fermi surface (see N. Andrei[39]), and therefore the approach is trustworthy only for very small voltages. Nevertheless, the dressed excitations framework seems to give at least qualitatively good results when another energy scale (such as the temperature or an external field) is turned on[40]. In contrast we construct the eigenstates of the Hamiltonian directly in terms of the bare electron field and can therefore impose the asymptotic boundary condition that the wave function tend to a product of two free Fermi seas composed of bare electrons. While we do not have a mathematically rigorous derivation of the weight functions we introduced, the validity of the scattering formalism is not restricted to any energy window other than energy cutoff.

C. Results for equilibrium and linear response

In the numerical computation, for the practical purpose, we assumed Kondo limit ($U = -2\epsilon_d$, $\frac{U}{\Gamma} \gg 1$) form of the spin-fluctuation and charge-fluctuation distributions, i.e.

$$D_s(\varepsilon(\lambda)) \simeq \frac{1}{\pi} \frac{T_k}{\varepsilon^2(\lambda) + T_k^2} \tag{18}$$

and

$$D_h(\varepsilon(\lambda)) \simeq \frac{1}{\sqrt{2U\Gamma}} \frac{\Gamma^2}{(\varepsilon(\lambda) + \epsilon_d)^2 + \Gamma^2} \tag{19}$$

with T_k being the Kondo scale derived in Ref. 36 as

$$T_k = \frac{\sqrt{2U\Gamma}}{\pi} e^{\pi \frac{\epsilon_d(\epsilon_d + U) + \Gamma^2}{2U\Gamma}} \,. \tag{20}$$

We also take $\varepsilon(\lambda) \simeq x(B) - x(\lambda)$ for numerical convenience with B denoting the Bethe momenta given by $\mu_1 = \mu_2 = 0$. The dot occupation $\langle \sum_\sigma d_\sigma^\dagger d_\sigma \rangle$ evaluated by these new phases is given by

$$\langle \sum_\sigma d_\sigma^\dagger d_\sigma \rangle = 2 \Bigg(\int_{B1}^\infty \mathrm{d}\lambda \, \sigma_b(\lambda)(\nu^s(\lambda) f_s(\lambda) + \nu^h(\lambda) f_h(\lambda)) + \int_{B_2}^\infty \mathrm{d}\lambda \, \sigma_b(\lambda)(\nu^s(\lambda) f_s(\lambda) + \nu^h(\lambda) f_h(\lambda)) \Bigg) \tag{21}$$

with $\nu^s(\lambda)$ and $\nu^h(\lambda)$ given as

$$\nu^s(\lambda) = \frac{1}{\Gamma} \left[1 - \frac{(\tilde{x}^2(\lambda) + y^2(\lambda) - \Gamma^2)}{\sqrt{(\tilde{x}^2(\lambda) + y^2(\lambda) - \Gamma^2)^2 + 4\Gamma^2 \tilde{x}^2(\lambda)}} \right] \times \left[1 + 8y(\lambda) \frac{1}{\Gamma} \left(1 - \frac{(\tilde{x}^2(\lambda) + y^2(\lambda) - \Gamma^2)}{\sqrt{(\tilde{x}^2(\lambda) + y^2(\lambda) - \Gamma^2)^2 + 4\Gamma^2 \tilde{x}^2(\lambda)}} \right) \left(\frac{\tilde{x}(\lambda)}{2\tilde{x}(\lambda) - U} \right)^2 \right] \tag{22}$$

$$\nu^h(\lambda) = \left[\frac{2\Gamma \tilde{x}^2(\lambda)}{(\tilde{x}^2(\lambda) + \Gamma^2)^2 - 2y^2(\lambda)(\Gamma^2 - \tilde{x}^2(\lambda)) + y^4(\lambda)} \right] \times \left[1 + \frac{36y(\lambda)\Gamma \tilde{x}^2(\lambda)}{(\tilde{x}^2(\lambda) + \Gamma^2)^2 - 2y^2(\lambda)(\Gamma^2 - \tilde{x}^2(\lambda)) + y^4(\lambda)} \left(\frac{\tilde{x}(\lambda)}{2\tilde{x}(\lambda) - U} \right)^2 \right] \tag{23}$$

respectively. We may check whether this choice of *phenomenological distribution functions* satisfy the condition in equilibrium that

$$\langle \sum_\sigma d_\sigma^\dagger d_\sigma \rangle = 4 \int_B^\infty \mathrm{d}\lambda \, \sigma_b(\lambda) \nu^{SBA}(\lambda) = 4 \left(\int_B^\infty \mathrm{d}\lambda \, \sigma_b(\lambda)(\nu^s(\lambda) f_s(\lambda) + \nu^h(\lambda) f_h(\lambda)) \right) \,. \tag{24}$$

We can see from the Top of Fig. 1 that the comparison between the phenomenological and the exact result for the dot occupation in equilibrium is good deep into the Kondo regime ($\epsilon_d \simeq -\frac{U}{2}$) and far away from it ($\epsilon_d \gg 0$) but is worse when we are in mixed valence region ($\epsilon_d \simeq 0$). This discrepancy, due in part to the approximations we made for $D_s(\varepsilon)$ and $D_h(\varepsilon)$, may go away if we took more realistic form of $D_s(\varepsilon(\lambda))$ and $D_h(\varepsilon(\lambda))$ also in mixed valence regime as suggested in Fig. 1. However the numerical procedure is much more complicated there. We confine ourself to this simpler limit in our phenomenological approach.

Another check on our result in equilibrium is to find the linear response conductance through our formulation and compare with the exact linear result given by the Friedel sum rule[25,26]. The Friedel sum rule, which relates the equilibrium dot occupation to the phase shift experienced by electrons crossing the dot, is related to zero voltage conductance by $\frac{dI}{dV}|_{V=0} = 2\sin^2(\pi\langle\hat{n}_d\rangle/2)$. The zero bias conductance in our construction can be analyzed easily[41] by noting that at low-voltage $eV = \mu_1 - \mu_2 \simeq \frac{2\pi}{L}(N_1 - N_2) = 4\pi\int_{B_1}^{B_2}\sigma_b(\lambda)d\lambda$. By taking $B_2 \simeq B_1 = B$ in the expression for the current across the impurity Eq. (12) we get the zero bias conductance expressed as

$$\frac{dI}{dV}\Big|_{V=0} = \frac{e^2}{h}\left[f_s(B)J^s(B) + f_h(B)J^h(B)\right] \qquad (25)$$

Here $B = B(\mu, \epsilon_d, \Gamma, U)$ is determined by $\mu_1 = \mu_2 = 0$. The comparison between Friedel sum rule (FSR) result and the conductance given by Eq. (25) (denoted as (pSBA)) is shown at the Bottom of Fig. 1. It displays the consequence of the equilibrium Kondo effect in the quantum dot set up: due to the formation of the Kondo peak attached to the Fermi level the Coulomb blockade is lifted and a unitary conductance is reached for a range of gate voltages ϵ_d around $-U/2$. Again we see that the comparison is good for large U/Γ but poorer in mixed valence regime for smaller U/Γ, which is consistent with the observation we made when evaluating $\langle\hat{n}_d\rangle$ as shown in top figure of Fig. 1. Having checked our results in equilibrium we shall go on to compute the current and the dot occupation in the out-of-equilibrium regime.

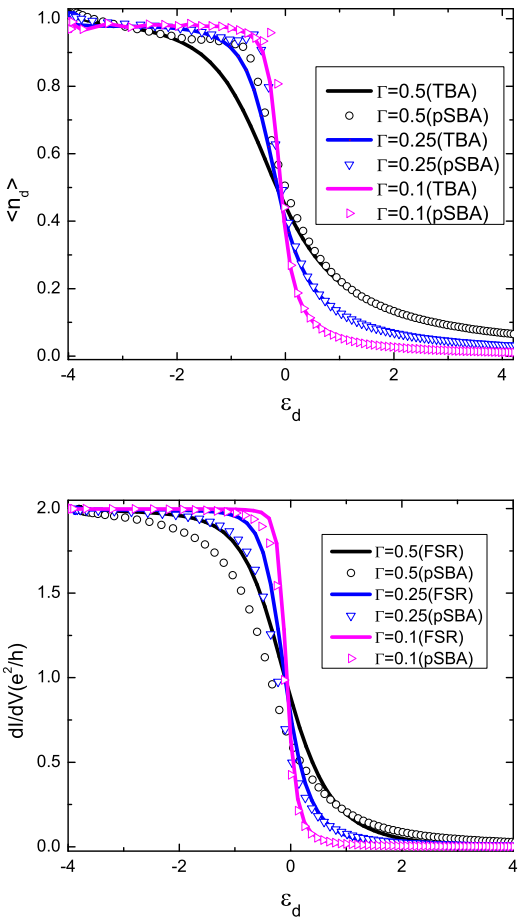

FIG. 1: Top: $\langle\hat{n_d}\rangle$ as a function of ϵ_d from the exact result (dotted line) and from Eq. (24) (solid line). Bottom: The differential conductance in the linear-response regime, as a function of ϵ_d from the phenomenological Scattering Bethe Ansatz (pSBA) and exact linear response conductance from Friedel sum rule (FSR) for $\Gamma = 0.5$, 0.25, 0.1, and $U = 8$.

D. Results Out-Of-Equilibrium

Now let us begin to investigate the current and dot occupation change as we turn on the voltage. We start with the discussion on current vs voltage for various regime. The current vs voltage is plotted in the inset of figure of Fig. 2 for different values of U and at the symmetric point $\epsilon_d = -U/2$. Note that we use an asymmetric bias voltage when solving numerically the integral equations originating from Eq. (5) with constraint of minimizing the charge free energy Eq. (6): Namely we fix $\mu_1 \simeq 0$ (around $10^{-3}-10^{-5}$) and lower μ_2. Therefore, a direct confrontation between the results obtained from real-time simulations of the Anderson model out-of-equilibrium[17,18,21] is difficult but the main features of our calculation match the predicted results: a linear behavior of the I-V characteristics at low-voltage, the slope being obtained from the FSR (2 in units of e^2/h at the symmetric point), and a non-monotonic behavior at higher voltage, the so-called non-linear regime. In particular, our calculations show clearly that the current will decrease as U/Γ is increased which is in agreement with other numerical approaches (e.g. cf Fig. 2 of Ref. 18 for a comparison).

The plots of the differential conductance vs source drain voltage for different dot levels, ϵ_d, tunneling strengths Γ and interaction strengths U are shown in Fig. 2 and Fig. 4. Two major features emerge from these plots: 1) A narrow peak around zero bias reaching maximal value of $2e^2/h$ (the unitary limit) for values of the gate voltage close to the symmetric point ($\epsilon_d \simeq -U/2$). 2) A broader peak developing at finite bias. The first peak is a non-perturbative effect identified as the many

body Kondo peak, characteristic of strong spin fluctuations in the system. But the broad peak is due to renormalized charge fluctuations around the impurity level. Notice the two features merge as the gate voltage, ϵ_d is raised from the Kondo regime, $\epsilon_d = -U/2$, to the mixed valence regime, $\epsilon_d = 0$, with the Kondo effect disappearing. As a function of the bias the various curves describing the Kondo peak for different values of the parameters can be collapsed onto a single universal function $\mathrm{d}I/\mathrm{d}V = \mathrm{d}I/\mathrm{d}V(V/T_k^*)$ as shown in Fig. 3. Here T_k^* is defined as

$$T_k^* = c_1 \frac{\sqrt{2U\Gamma}}{\pi} e^{\frac{\epsilon_d(\epsilon_d+U)+\Gamma^2}{2U\Gamma}} \tag{26}$$

with $c_1 = 0.002$. The energy scale T_k^* was extracted from the numerics by requiring that the function $\mathrm{d}I/\mathrm{d}V(V/T_k^*)$ decreases to half its maximal value when $V \simeq T_k^*$. The expression for T_k^* as given by Eq. (26) differs from the thermodynamic T_k as defined in Eq. (20). The difference of prefactor in the exponential is certainly related to the unusual choice of regularization scheme in the SBA[34]. The other possible implication for this different formulation for the Kondo scale is also addressed later when we discuss the experiment done by L. Kouwenhoven et al[5].

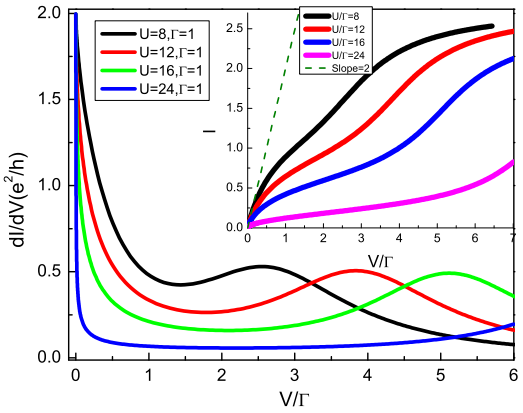

FIG. 2: dI/dV vs V/Γ for $\Gamma = 1$, $\epsilon_d = -U/2$, and various U. Inset: Steady state current vs voltage curves for $\Gamma = 1$, $\epsilon_d = -U/2$, and various U. Dashed line is a line with constant conductance $\frac{2e^2}{h}$ plotted for comparison.

The small voltage behavior for differential conductance in symmetric case, i.e. $\epsilon_d \simeq -\frac{U}{2}$, is expected to be[11,14]

$$\frac{dI}{dV}\Big|_{V \ll T_k^*} \simeq \frac{2e^2}{h}\left(1 - \alpha_V \left(\frac{V}{T_k^*}\right)^2\right)$$

and allows us to identify the constant α_V from the quadratic deviation from $2e^2/h$. The quadratic fit of the universal curve around $V \simeq 0$, as shown in Fig. 3, gives

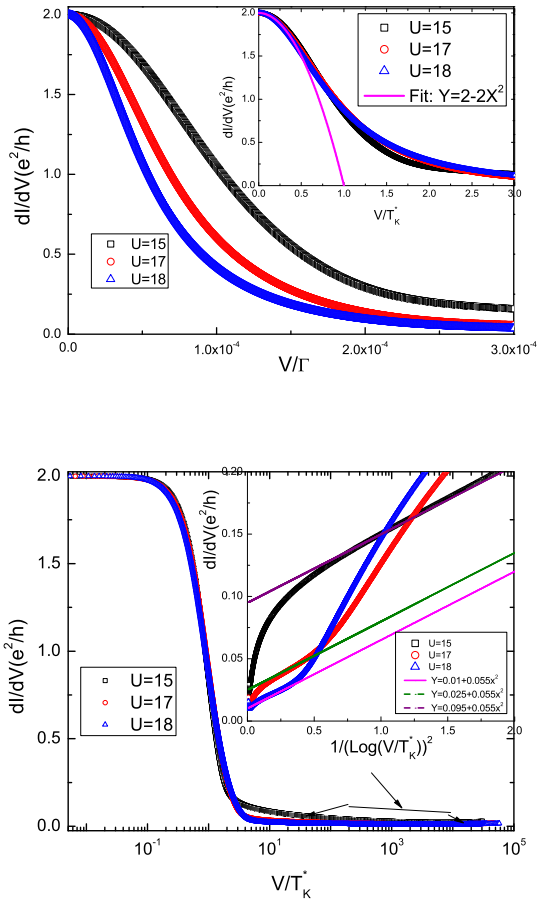

FIG. 3: Top: Zoomed in picture of the differential conductance vs voltage nearby zero voltage. Inset shows the universality in conductance vs voltage scaled by T_k^* when $\frac{V}{T_k^*} \leq 1$. The quadratic behavior occurs for $\frac{V}{T_k^*} < 0.5$ as indicated by the fitted curve. Bottom: Differential conductance vs voltage scaled by T_k^* nearby the Kondo peak structure. Inset shows the logarithmic behavior when $\frac{V}{T_k^*} \gg 1$. $\Gamma = 0.5$ for all these data sets.

$\alpha_V \simeq 1$. It is also expected for $T_k^* \ll V \ll \frac{U}{2}$ that the tail of the peak decays logarithmically [11] as

$$\frac{dI}{dV} \sim \frac{2e^2}{h} \frac{1}{\ln^2(\frac{V}{T_k^*})} .$$

The latter behavior is observed (see inset of Fig. 3) in the regime $\frac{U}{\Gamma} \gg 1$ for $10^2 < \frac{V}{T_k^*} < 10^4$ with the logarithmic function given by

$$\frac{dI}{dV} = \frac{e^2}{h}\left[f\left(\frac{U}{\Gamma}\right) + \frac{c_2}{\ln^2(\frac{V}{T_k^*})}\right]$$

with the parameter $c_2 = 0.055$. Here $f(\frac{U}{\Gamma})$ is simply a constant (in V) shift. As suggested from the bottom

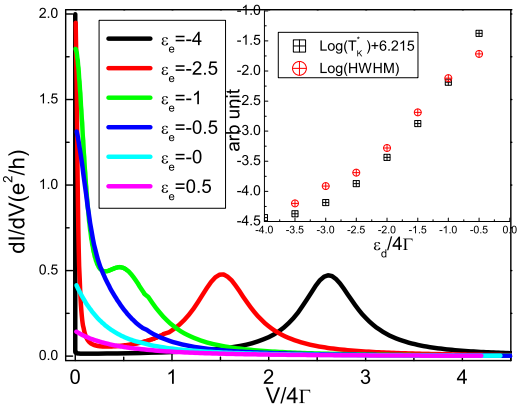

FIG. 4: dI/dV vs $V/4\Gamma$ for $U = 8$, $\Gamma = 0.25$ and various ϵ_d from Kondo ($\epsilon_d = -4$) to mixed valence regime ($\epsilon_d \simeq 0$). Inset: Comparison of $\ln(T_k^*) - \ln(c_1)$ and $\ln(V_{HWHM})$ as a function of impurity level ϵ_d. Here V_{HWHM} is the voltage difference estimated at half value of differential conductance at zero voltage. The constant shift $-\ln(c_1)$ is chosen to give the best fit in the data away from $\epsilon_d = -\frac{U}{2}$.

plot of Fig. 3 (see also Fig. 13 for the infinite U case) the charge fluctuation side peak does not fall into the same scaling relation but the strong correlations shift the center of the side peak closer to $V = 0$ (see Fig. 2 and Fig. 4). In other words the position of the resonance in the dI/dV curve naively expected around $V = |\epsilon_d|$ is renormalized[42] by the presence of interactions. In the inset of Fig. 4 we show the logarithm of the voltage obtained at half width half maximum (HWHM) of the zero voltage peak and compare it with

$$\ln T_k^* = \frac{\epsilon_d(\epsilon_d + U) + \Gamma^2}{2U\Gamma} + \ln\left(c_1 \frac{\sqrt{2U\Gamma}}{\pi}\right)$$

(after subtracting the constant $\ln c_1$). What is important and *universal* is that both quantities ($\ln V_{\rm HWHM}$ and $\ln T_k^*$) exhibit a quadratic behavior in the gate voltage ϵ_d. Similar results had been found experimentally by L. Kouwenhoven et al[5] when they compare the full width half maximum of dI/dV (from which they obtain a Kondo scale T_{k_1} at finite voltage) with the temperature dependence of the linear response differential conductance (from which another Kondo scale T_{k_2} is extracted). It is suggested from our numerical results that both $\ln T_{k_2}$ (in analogy with our T_k) and $\ln T_{k_1}$ (which is our T_k^*) follows similar quadratic behavior in ϵ_d but differ in their curvatures by a factor of π. In Ref. 5 the curvatures of the quadratic behavior differ by a factor of around 2 (see Fig.3B in Ref. 5) which is attributed to dephasing of spin fluctuations at finite voltage.

Notice that in all the numerical data shown for current vs voltage we have chosen $\frac{U}{\Gamma} \geq 8$ to explore the scaling relation in the Kondo regime. Another reason is that our *phenomenological distribution functions* introduced to control the relative weight for spin- and charge-fluctuation contributions work is much better in the large $\frac{U}{\Gamma}$ regime (cf. Fig. 1).

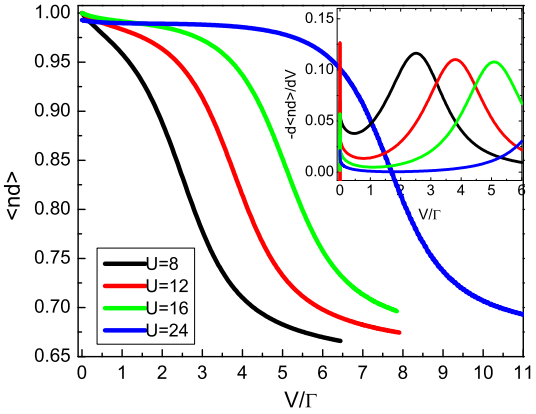

FIG. 5: $\langle \hat{n_d} \rangle$ vs V/Γ for different U with $\epsilon_d = -\frac{U}{2}$ and $\Gamma = 1$ case. Inset: The corresponding nonequilibrium charge susceptibility. A small peak shows up nearby $V = 0$ for all these curves.

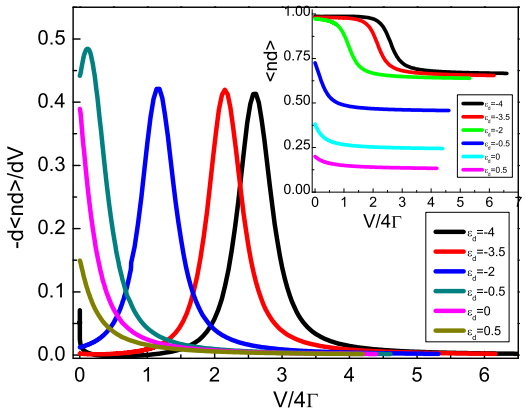

FIG. 6: $-\frac{d\langle \hat{n}_d \rangle}{dV}$ vs $V/4\Gamma$ for $\Gamma = 0.25$, $U = 8$, and various ϵ_d from Kondo to mixed valence regime. We see that the small peak nearby $V = 0$ only appears when $\epsilon_d \to -\frac{U}{2}$. Inset: The corresponding $\langle \hat{n_d} \rangle$ vs $V/4\Gamma$.

Next let us study the change in the dot occupation as a function of the voltage. The extension of the computation of the dot occupation out of equilibrium is straightforward. Suppose we find the correct distribution functions $f_s(\lambda)$ and $f_h(\lambda)$ then we have $\nu^{SBA}(\lambda) = \nu^s(\lambda) f_s(\lambda) + \nu^h(\lambda) f_h(\lambda)$. Under this assumption $\nu^{SBA}(\lambda)$ retains its form in and out-of-equilibrium and the general

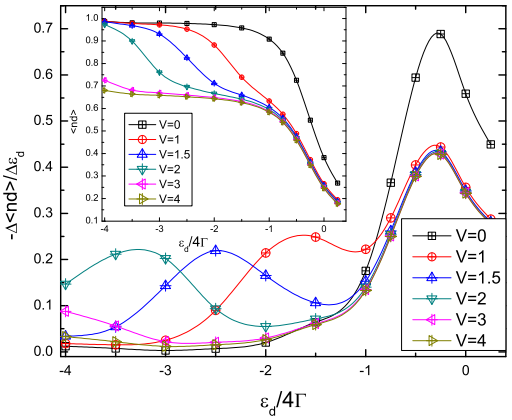

FIG. 7: $-\frac{\Delta\langle\hat{n}_d\rangle}{\Delta\epsilon_d}$ for various fixed voltages as a function of ϵ_d for $\Gamma = 0.25$, $U = 8$. Inset shows $\langle\hat{n}_d\rangle$ vs ϵ_d for various fixed voltage.

expression for $\langle\hat{n}_d\rangle$ is

$$n_d(\mu_1,\mu_2) = \langle\Psi,\mu_1,\mu_2|\hat{n}_d|\Psi,\mu_1,\mu_2\rangle \qquad (27)$$
$$= 2\left(\int_{B_1}^{\infty} \mathrm{d}\lambda\ \sigma_b(\lambda)\nu^{SBA}(\lambda) + \int_{B_2}^{\infty} \mathrm{d}\lambda\ \sigma_b(\lambda)\nu^{SBA}(\lambda)\right)$$

As the form for $\nu^{SBA}(\lambda)$ is proved to be *exact* in equilibrium, we shall regard Eq. (27) as an *exact* result for $\langle\hat{n_d}\rangle$ in and out of equilibrium and valid in all different range of U, ϵ_d, Γ. In the numerical results shown hereafter we shall use this *exact* expression, Eq.(27), for matrix element of dot occupation rather than Eq. (24). We adopt the same voltage drive scheme by fixing μ_1 and lowering μ_2.

By using this *exact* result we do not need to confine ourself for large $\frac{U}{\Gamma}$. The case for different $\frac{U}{\Gamma}$ with $\epsilon_d = -\frac{U}{2}$ and for $U = 8, \Gamma = 0.25$ with different ϵ_d are shown in Fig. 5 and Fig. 6. The main features of these plots are a relatively slow decrease of the dot occupation at low voltage followed by an abrupt drop of $\langle n_d\rangle$. The decrease of $\langle n_d\rangle$ takes place within a range of voltage of the order of Γ. Then as we increase the voltage further another plateau develops. Note that, as expected, the bigger U is the higher the voltage needed to drive the system out of the $\langle n_d\rangle = 1$ plateau. In a sense the charge fluctuations are strongly frozen at large U and it costs more energy to excite them. The voltage where the abrupt drop in $\langle n_d\rangle$ occurs corresponds to the energy scale at which the "charge fluctuation peak" was observed in the conductance plots. This can be seen by comparing the position of the broader peak in Fig. 4 with that of the abrupt dot occupation drop in Fig. 6.

Similar to the differential conductance we may define the *nonequilibrium charge susceptibility* as

$$\chi_c(V)|_{\epsilon_d} = -\frac{\partial\langle\hat{n_d}\rangle}{\partial V}$$

that we obtain by taking a numerical derivative of the dot occupation data with respect to the voltage. In the case of $U = -\epsilon_d/2$ there are two features as can be seen from the inset of Fig. 5 and main figure of Fig. 6. Nearby $V \simeq 0$ we see a first small peak arising with width and height decreasing with increasing $\frac{U}{\Gamma}$. We identify this peak as a small remnant of the charge fluctuations in the Kondo regime. This statement is confirmed by noticing that this peak goes away as $\frac{U}{\Gamma}$ increases, vanishing when $U \to \infty$ as shown in Section III where the infinite U Anderson model is discussed. The second peak is located at the same voltage as the charge fluctuation peak observed in the conductance plots and is therefore associated to the response of the renormalized impurity level to the charge susceptibility. This can be seen when comparing Fig. 4 and Fig. 6.

Another interesting quantity, the usual *charge susceptibility*, defined by $\chi_c(\epsilon_d)|_V = -\frac{\partial\langle\hat{n_d}\rangle}{\partial\epsilon_d}$, can also be qualitatively described. In Fig. 7 we plot $-\frac{\Delta\langle\hat{n_d}\rangle}{\Delta\epsilon_d}$ as a function of ϵ_d as we only have a few points in fixed ϵ_d for finite voltage. Notice that $\chi_c(\epsilon_d)|_V$ tends to be an universal curve in large voltage, indicating charge on the dot remains at some constant value in the steady state with large voltage. This constant value at large voltage, as pointed out by C. J. Bolech, is around 0.65 for $\epsilon_d = -\frac{U}{2}$ case. In preparing this article we noticed that a similar computation, adopting the same asymmetric voltage drive protocol as we have here, is carried out by R. V. Roermund et al[19] for the dot occupation out of equilibrium by using equation of motion method. We do get a similar value for the dot occupation at large voltage. This value is different from the dot occupation value $n_d \simeq 0.5$ at large voltage when the interaction U is turned off as shown in Fig. 12. This difference might have to do with the 0.7 structure observed in quantum point contact[4] in high temperature (temperature is high compared with the Kondo scale but still small compared with phonon modes or electronic level) and zero magnetic field as the linear response conductance given by $n_d = 0.65$ by using Friedel sum rule is around 0.73. In a sense the voltage seems to play a similar role to the temperature on the way it influences the dot occupation. Further connection between these two behaviors could be clarified by computing the decoherence factor as in Ref. 19. This decoherence factor is related to the dot correlation function out of equilibrium which can be computed in three-lead setup[47] by using our approach.

E. Comparison with other theoretical and experimental results

In most of the other theoretical approaches[16–20,27,28] the symmetric voltage drive ($\mu_1 = -\mu_2$) is usually assumed to preserve particle-hole symmetry in symmetric case ($\epsilon_d = -\frac{U}{2}$). It is thus difficult for us to make any definite comparison with other theoretical results. The qualitative feature, as shown by the black curves in Fig. 8

done by D. Matsumoto[20] by using perturbation expansion in U at strong coupling fixed point, is similar to our results in the sense that the height of the charge fluctuation side peak and width are almost the same. The major differences are in the shape of Kondo peak and the position of the charge fluctuation side peak. A clear signature of renormalized dot level ϵ_d as hinted in renormalization computation[42,43] is clearly seen in our result. The shape of Kondo resonance nearby zero voltage deviates from its quadratic behavior expected from Fermi liquid picture at smaller voltage in our case as is expected for asymmetric voltage drive[13,15].

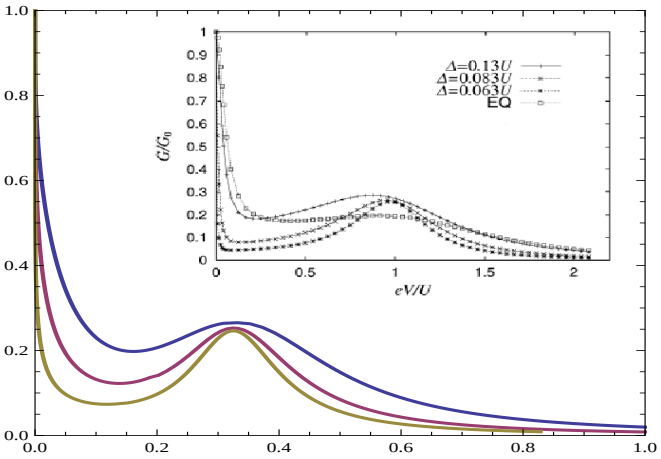

FIG. 8: Comparison of our theory with perturbation expansion in U done by D. Matsumoto on dI/dV (y-axis in unit of $2e^2/h$) vs V/U (x-axis). Our data (Blue, purple, and brown lines correspond to $\frac{\Gamma}{U} = 0.13, 0.083, 0.063$ respectively. Δ shown in inset is Γ in our notation. EQ in the inset is conductance computed by equilibrium density of state which is not relevant to our discussion here.) is shown as the main figure and Fig.8 in Ref 20 is shown in the inset. In Ref 20 the voltage is driven symmetrically, i.e. $\mu_1 = -\mu_2$, rendering the factor of two difference in the voltage (i.e. $\frac{V}{U} = 0.5$ in our case corresponds to $\frac{eV}{U} = 1$ in the inset. $e = 1$ in our convention.) in comparing our result with that in Ref 20.

We can also compare our results with experiments. As shown in the inset of Fig. 9 is the $\frac{dI}{dV}$ vs V measured in Co ion transistor by J. Park et al.[6]. We rescaled the differential conductance and superimposed our numerical results on the data graph. The measurement was done by using an asymmetric drive of the voltage (by keeping $\mu_1 = 0$ and changing μ_2 to be larger or smaller than zero) and thus there is an asymmetry in the differential conductance as a function of voltage as illustrated in the data curve. In our numerics we only compute the scenario for $\mu_1 = 0$ and lowering μ_2 (only for $V > 0$ region of Fig. 9). The $V < 0$ region is plotted by just a reflection with respect to the $V = 0$ axis which illustrates the case of $\mu_2 = 0$ and lowering μ_1. To compare with the correct voltage setup on the $V < 0$ side as in experiment will involve computations within a different parametrization for bare the Bethe momenta which is beyond our current

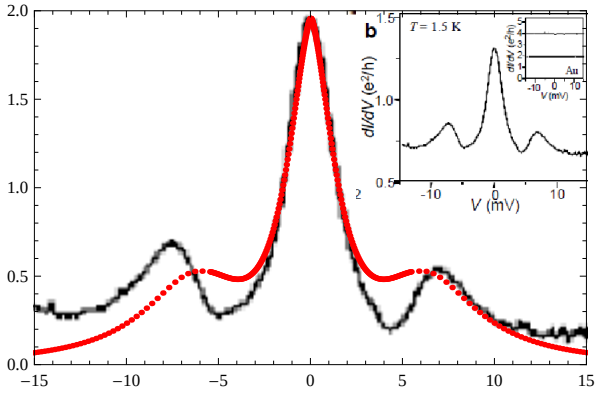

FIG. 9: Comparison of theory with experiment of dI/dV (y-axis in unit of e^2/h) vs V (x-axis in unit of mV). Inset is the original data graph published in Ref. 6. The red dots are given by our theory for $\frac{U}{\Gamma} = 8$ with voltage rescaled to fit with original data in unit of mV. The value of differential conductance (experiment data in black line) is rescaled from $(0.6, 1.3)$ to $(0, 2)$ in unit of $\frac{e^2}{h}$.

scope. The comparison on the $V > 0$ region shows good agreement between our theory and experimental result. The discrepancy on the width of the charge fluctuation side peak could be due to the vibron mode[44]. To describe these type of transistors we shall start with the Anderson-Holstein Hamiltonian. We are currently exploring the possibility of solving this model by the Bethe Ansatz approach.

III. INFINITE U ANDERSON MODEL

In the limit of $\frac{U}{\Gamma} \to \infty$ the finite U two-lead Anderson impurity Hamiltonian becomes the two-lead infinite U Anderson model. The latter model is closely related, via the Schrieffer-Wolff transformation[45], to the notorious Kondo model, a model of spin coupled to a Fermi liquid bath. The reason for that is simple: since $U \to \infty$ the charge fluctuations are essentially frozen out and only the spin fluctuations dominate the low-energy physics. The Hamiltonian is given by

$$\hat{H} = \sum_{i=1,2} \int \mathrm{d}x\, \psi^\dagger_{i\sigma}(x)(-i\partial_x)\psi_{i\sigma}(x) + \epsilon_d d^\dagger_\sigma d_\sigma + t_i(\psi^\dagger_{i\sigma}(0)b^\dagger d_\sigma + d^\dagger_\sigma b\psi_{i\sigma}(0)) \quad (28)$$

Here the bosonic operator b is introduced to conserve $b^\dagger b + \sum_\sigma d^\dagger_\sigma d_\sigma = 1$ and by applying the slave boson technique we project out the phase space of double occupancy occurring in finite U case. The corresponding Bethe momenta distribution function for the infinite U Anderson

model is given by

$$2\sigma(\Lambda) = \frac{1}{\pi} - \int_{-\infty}^{B_2} d\Lambda' K(\Lambda-\Lambda')\sigma(\Lambda') - \int_{-\infty}^{B_1} d\Lambda' K(\Lambda-\Lambda')\sigma(\Lambda') \quad (29)$$

with $K(\Lambda) = \frac{1}{\pi}\frac{2\Gamma}{(2\Gamma)^2+(\Lambda-\Lambda')^2}$.

Eq. (29) can be derived directly following the procedures in the finite U Anderson model. It can also be derived from the finite U result, Eq. (5), by taking the large U limit ($U \gg \epsilon_d$, $U \gg \Gamma$):

$$\begin{aligned}
\frac{x(\lambda)}{U} &\to \frac{1}{2} - \sqrt{\frac{\frac{\lambda}{U^2}+\frac{1}{4}+\sqrt{(\frac{\lambda}{U^2}+\frac{1}{4})^2+\frac{\Gamma^2}{U^2}}}{2}} \\
&\to \frac{1}{2} - \sqrt{\frac{\frac{\lambda}{U^2}+\frac{1}{4}+|\frac{\lambda}{U^2}+\frac{1}{4}|}{2}} \quad (30) \\
&\to \frac{1}{2} - \frac{1}{2}(1+\frac{2\lambda}{U^2}+\ldots) \to -\frac{\lambda}{U^2} = \frac{\Lambda}{U} \\
\frac{y(\lambda)}{U} &\to \sqrt{\frac{-(\frac{\lambda}{U^2}+\frac{1}{4})+((\frac{\lambda}{U^2}+\frac{1}{4})^2+\frac{\Gamma^2}{U^2})^{1/2}}{2}} \\
&\to \sqrt{\frac{(\frac{\lambda}{U^2}+\frac{1}{4})(-1+(1+\frac{(\frac{\Gamma}{U})^2}{(\frac{\lambda}{U^2}+\frac{1}{4})^2})^{1/2})}{2}} \quad (31) \\
&\to \left(\frac{1}{4}\frac{(\frac{\Gamma}{U})^2}{\frac{1}{4}}\right)^{1/2} + \mathcal{O}(U^{-2}) \simeq \frac{\Gamma}{U}
\end{aligned}$$

with $\Lambda \equiv -\frac{\lambda}{U}$. Similar procedures as in Appendix C give the matrix element $\nu_\infty^{SBA}(\Lambda)$ for the dot occupation in the infinite U Anderson model in equilibrium to be

$$\nu_\infty^{SBA}(\Lambda) = \frac{2\Gamma}{(\Lambda-\epsilon_d)^2+(2\Gamma)^2} \ . \quad (32)$$

In going to the out-of-equilibrium regime ($\mu_1 \neq \mu_2$) we follow the same phenomenological method as for the finite U case. The result for the spin-fluctuation and charge-fluctuation contributions to the dot occupation are given by

$$\begin{aligned}
\nu_\infty^s(\Lambda) &= \frac{1}{\Gamma}\left(1 - \frac{\epsilon_d-\Lambda}{\sqrt{(\epsilon_d-\Lambda)^2+4\Gamma^2}}\right) \\
\nu_\infty^h(\Lambda) &= \frac{2\Gamma}{(\Lambda-\epsilon_d)^2+(2\Gamma)^2} \ . \quad (33)
\end{aligned}$$

We shall again check the consistency with the exact result for the dot occupation in equilibrium, namely

$$\begin{aligned}
\langle \sum_\sigma d_\sigma^\dagger d_\sigma \rangle &= 4\int_D^B \mathrm{d}\Lambda\ \sigma_b(\Lambda)\nu_\infty^{SBA}(\Lambda) \\
&= 4\int_D^B \mathrm{d}\Lambda\ \sigma_b(\Lambda)(\nu_\infty^s(\Lambda)f_s^\infty(\Lambda) + \nu_\infty^h(\Lambda)f_h^\infty(\Lambda)) \ .
\end{aligned}$$

Here D is related to the bandwidth and B is determined by the equilibrium Fermi energy $\mu_1 = \mu_2 = 0$. $f_s^\infty(\Lambda)$ and $f_h^\infty(\Lambda)$ are expressed as

$$\begin{aligned}
f_s^\infty(\Lambda) &= \frac{T_k^\infty/\pi}{(\Lambda-B)^2+(T_k^\infty)^2} \\
f_h^\infty(\Lambda) &= \frac{2\Gamma}{(\Lambda-B-\epsilon_d)^2+(2\Gamma)^2} \ .
\end{aligned}$$

Here the Kondo scale T_k^∞ used in $f_s(\Lambda)$ takes the form[46]

$$T_k^\infty = \frac{\sqrt{10|D|\Gamma}}{\pi} e^{-\pi\frac{|\epsilon_d|}{\Gamma}} \ .$$

The results for the dot occupation and Friedel sum rule check in the infinite U case are shown in Fig.10. Again we see a nice match between our phenomenological approach and the exact result for $|\frac{\epsilon_d}{\Gamma}| \neq 0$ and some mismatch in the mixed valence region $|\frac{\epsilon_d}{\Gamma}| \simeq 0$. This is consistent with the results for finite U.

The corresponding spin and charge fluctuation matrix element for current, $J_\infty^s(\Lambda)$ and $J_\infty^h(\Lambda)$, are given by

$$\begin{aligned}
J_\infty^s(\Lambda) &= 1 - \frac{\epsilon_d-\Lambda}{\sqrt{(\epsilon_d-\Lambda)^2+4\Gamma^2}} \\
J_\infty^h(\Lambda) &= \frac{2\Gamma^2}{(\Lambda-\epsilon_d)^2+(2\Gamma)^2} \quad (34)
\end{aligned}$$

The current expectation value is given by

$$\langle \hat{I} \rangle = \frac{2e}{\hbar}\int_{B_2}^{B_1} d\Lambda\sigma(\Lambda)(J_\infty^s(\Lambda)f_s^\infty(\Lambda) + J_\infty^h(\Lambda)f_h^\infty(\Lambda))$$

where B_1 and B_2 are related to μ_1 and μ_2 by minimizing charge free energy F

$$F = 2\left(\int_D^{B_1} \mathrm{d}\Lambda\,\sigma(\Lambda)(\Lambda-\mu_1) + \int_D^{B_2} \mathrm{d}\Lambda\,\sigma(\Lambda)(\Lambda-\mu_2)\right) \ .$$

Before we proceed to discuss the numerical results for current vs voltage in this infinite U model let us look at the structure of $J_\infty^s(\Lambda)$ and $J_\infty^h(\Lambda)$ as a function of Λ as shown in Fig. 11. Λ here represents the bare energy of the quasi-particle and plays the same role as $x(\lambda)$ in the finite U Anderson model. $J_\infty^s(\Lambda)$ alone would reproduce the main feature in the Friedel sum rule for $\epsilon_d \ll 0$. In this region the linear response conductance comes mainly from the spin fluctuations. The upper plot of Fig. 11 fixes ϵ_d and shows $J_\infty^s(\Lambda)$ vs Λ. We may also fix $\Lambda = 0$ (in the sense of choosing the equilibrium Fermi surface energy at $\Lambda = 0$) and plot $J_\infty^s(\epsilon_d)$ vs ϵ_d. In this way we can see that $J_\infty^s(\epsilon_d)$ vs ϵ_d reproduces the overall structure of the linear response conductance from the Kondo region ($\epsilon_d \leq 0$) to the mixed valence regime ($\epsilon_d \simeq 0$). Therefore we identify the phase shift $\frac{\delta_{p^+}+\delta_{p^-}}{2}$, contributing to $J_\infty^s(\Lambda)$, as the phase shift related to spin-fluctuation.

$J_\infty^h(\Lambda)$ gives a Lorentz shape in bare energy scale Λ. This structure is akin to the charge fluctuation side peak

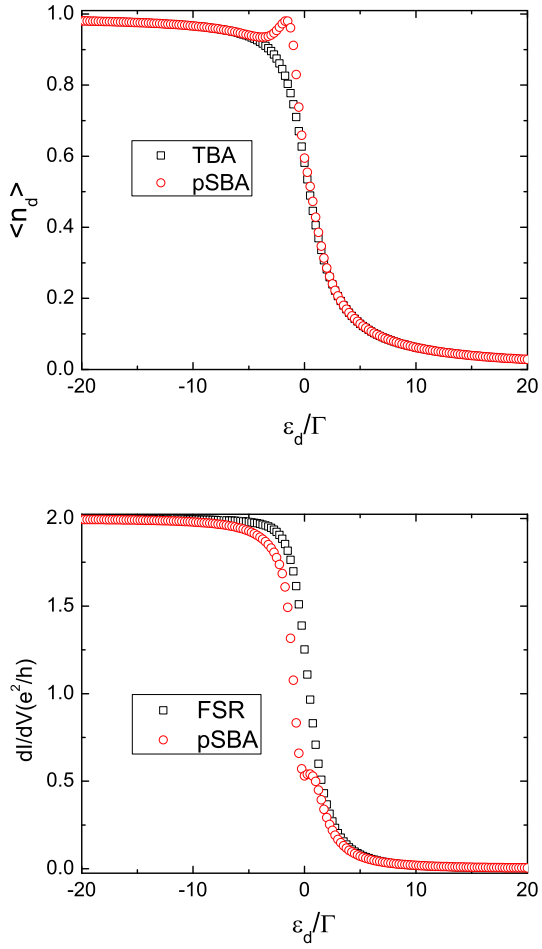

FIG. 10: Top: $\langle \hat{n}_d \rangle$ vs $\frac{\epsilon_d}{\Gamma}$ for exact TBA result and pSBA. Bottom: Linear response conductance $dI/dV|_{V\to 0}$ vs $\frac{\epsilon_d}{\Gamma}$ for exact result (FSR) and pSBA in the infinite U Anderson model. $\frac{D}{\Gamma} = -100$. Similar to the case of finite U the comparison nearby mixed valence region ($\epsilon_d \simeq 0$) is poorer.

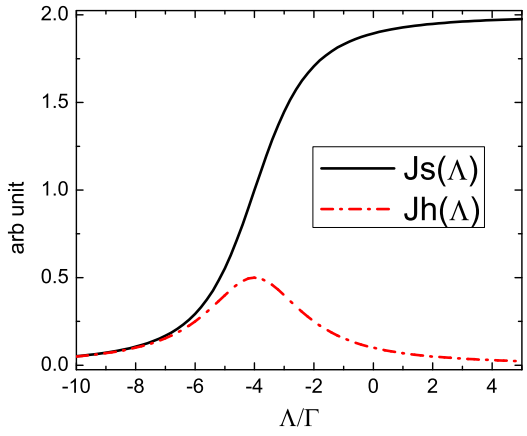

FIG. 11: $J_s(\Lambda)$ and $J_h(\Lambda)$ vs Bethe momenta Λ (scaled by Γ) in infinite U Anderson model. $\frac{\epsilon_d}{\Gamma} = -4$ in this graph. Similar graph appears for finite U case with x-axis replaced by real part of Bethe momenta $x(\lambda)$.

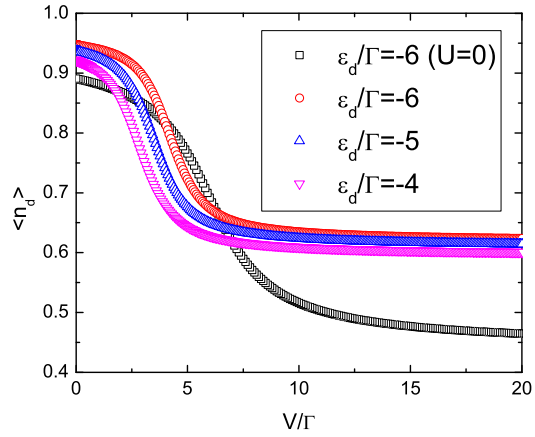

FIG. 12: $\langle \hat{n}_d \rangle$ vs $\frac{\epsilon_d}{\Gamma}$ in infinite U Anderson model (for Red, Blue, and Purple dots. The Black dots are $U = 0$ case shown for comparison). $\frac{D}{\Gamma} = -100$ in this graph.

with peak position at energy scale around ϵ_d as seen from lower plot of Fig. 11. Thus we identify the phase shift $\delta_{p^+} + \delta_{p^-}$, contributing to $J^h_\infty(\Lambda)$, as the phase shift related to charge-fluctuation. These structures also apply to the case of the finite U Anderson model.

Now let us discuss the out of equilibrium numerical results. The voltage is again driven asymmetrically by fixing $\mu_1 \simeq 0$ and lowering μ_2. The *exact* dot occupation vs voltage for different ϵ_d for infinite U and $U = 0$, $\frac{\epsilon_d}{\Gamma} = -6$ case (black dots) are shown in Fig. 12. We see again the dot occupation decreases slowly at low voltage and develops an abrupt drop at a voltage scale corresponding to impurity level ϵ_d. Also notice the apparent difference between the $U = 0$ plot (black dots) and the $U \to \infty$ case (red dots) and for the same value of $\frac{\epsilon_d}{\Gamma}$. For $U \to \infty$, the dot occupation at large voltage is around 0.65 for $\frac{\epsilon_d}{\Gamma} \ll 0$ which is consistent with the result of the finite U case when $\frac{U}{\Gamma}$ is large (cf. Section II D). In contrast the non-interacting case ($U = 0$) shows that $\langle n_d \rangle \to 0.5$ at large bias.

The *phenomenological* current vs voltage and the corresponding differential conductance vs voltage are plotted in the top figure of Fig. 13. Again we see the zero bias anomaly and a broad charge fluctuation side peak in the differential conductance vs voltage. The scaling relation of differential conductance vs voltage expected in small voltage region can also be extracted by rescaling the voltage by $T_k^{\infty *}$ as shown in bottom figure of Fig. 13. Here $T_k^{\infty *}$ is given by

$$T_k^{\infty *} = \frac{\sqrt{10|D|\Gamma}}{\pi} e^{-\pi \frac{|\epsilon_d|}{2\Gamma}} \ .$$

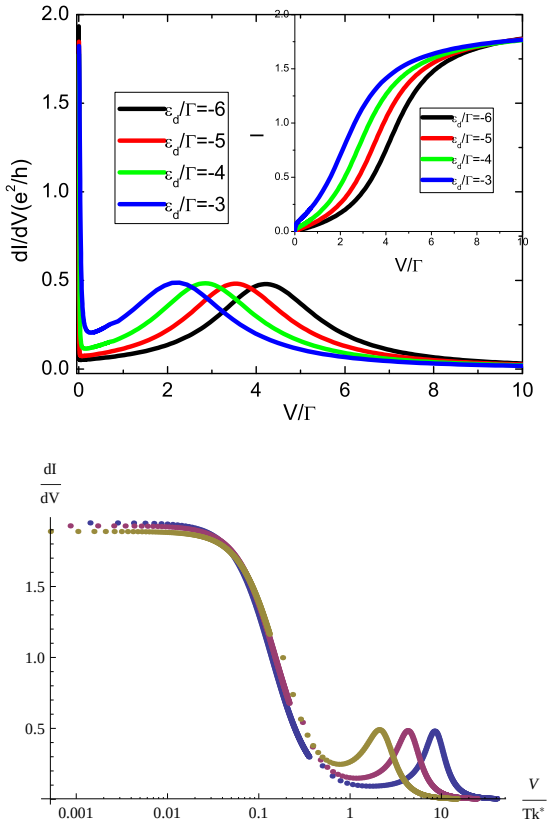

FIG. 13: Top: $\frac{dI}{dV}$ vs $\frac{V}{\Gamma}$ in infinite U Anderson model. Inset shows the $I-V$ curves for these parameters. $\frac{D}{\Gamma} = -100$ in this graph. Bottom: $\frac{dI}{dV}$ vs $\frac{V}{T_k^*}$ shows the scaling relation nearby zero voltage for $\frac{\epsilon_d}{\Gamma} = -6, -5, -4$ (Blue, Purple, Brown).

Notice this $T_k^{\infty *}$ differs from T_k^{∞} with a factor of two within the exponent. This factor of two difference represents the difference in the curvature of the parabola as function of ϵ_d (the logarithm of half width at half maximum of the Kondo peak vs ϵ_d shows parabolic curve as in inset of Fig. 5 for finite U case). This factor of two ratio bears even closer resemblance to the results shown in Ref. 5. Note that in bottom figure of Fig. 13 the positions of the side peak are different and show no universality in that region. It shows universality for $\frac{V}{T_k^*} \leq 1$.

IV. CONCLUDING REMARKS

In this article we have explicitly computed the non-equilibrium transport properties in the Anderson model for all voltages using the Scattering Bethe Ansatz. In the case of equilibrium we have also shown the equivalence of traditional Bethe Ansatz and Scattering Bethe Ansatz by evaluating dot occupation in equilibrium. For the expression of current we have introduced *phenomenological distribution functions* to set the weight for spin-fluctuation and charge-fluctuation contributions to the current. The result shows correct scaling relation in Kondo regime as well as satisfying the Friedel sum rule for linear response for large $\frac{U}{\Gamma}$.

Other interesting quantities, such as the *nonequilibrium charge susceptibility* or the usual charge susceptibility, are computed numerically via *exact* expression for dot occupation as a function of voltage and impurity level. We believe this is the first report of an *exact* computation of the dot occupation out-of-equilibrium and it may have interesting application in quantum computing as we understand more the dephasing mechanism. We have also compared our results with perturbation calculation and experimental measurement of nonlinear differential conductance of a quantum dot.

The major difficulty we encounter by using SBA comes from the single particle phase shift for complex momenta which leads to a breakdown of steady state condition when out of equilibrium. One possible issue resulting in this is the local discontinuity at odd channel s_{op}, the choice we made to enable us to construct a scattering state with fixed particles from lead 1 and lead 2. It can be proved that without this choice we cannot write down fixed number of particles incoming from each lead[35] in this Anderson impurity model and similarly for IRLM. The other issue in the study for Anderson model is whether we shall include all possible bound states in the ground state construction. From the mathematical structure we shall choose 4 type of bound states but the results from charge susceptibility seems to suggest 2 type of bound states is the correct choice. To check whether this is in general correct we plan to come back to study the whole spectrum, which include bound state when Bethe energy higher than impurity level, of IRLM as this model bares structure similarity to the Anderson model described in this article. Following the SBA on IRLM[7] there are lots of numerical approach and different exact methods[23] developed for this model and detailed comparison for different approaches is desired for better understanding its physics and scaling relation. By learning how to deal with complex momenta in this model we may also find the rule which may lead us to the *exact* expression for current in this Anderson impurity model.

Acknowledgment

We are grateful to Kshitij Wagh, Andres Jerez, Carlos Bolech, Pankaj Mehta, Avi Schiller, Kristian Haule, and Piers Coleman for many useful discussions and most particularly to Chuck-Hou Yee for his important help with the numerics and to Natan Andrei for numerous discussions and fruitful ideas. S. P. would also like to thank Daniel Ralph and Joshua Park for permission to use their data and discussion. G. P. acknowledges support from the Stichting voor Fundamenteel Onderzoek der Materie (FOM) in the Netherlands. This research was supported in part by NSF grant DMR-0605941 and DoEd GAANN

fellowship.

Appendix A: Discussion of 2 strings vs 4 strings

As we have discussed in the main text the bounded pair, formed by $p^{\pm}(\lambda) = x(\lambda) \mp iy(\lambda)$, can be formed by quasi-momenta from lead 1 or lead 2. We have shown the results for two type of strings (bound states). Namely the strings are formed by $\{ij\} = \{11, 22\}$ with i, j denoting incoming lead indices. In this section we discuss the case of 4 type of strings and show thier corresponding numerical results in out of equilibrium regime (In equilibrium the 2 strings and 4 strings give the same result for dot occupation).

The density distribution for the Bethe momenta (rapidities) is denoted by $\sigma_{ij}(\lambda)$ with $\{ij\} = \{11, 12, 21, 22\}$ indicating the incoming electrons from lead i and lead j. The $\sigma_{ij}(\lambda)$ is given by

$$4\sigma_{ij}(\lambda) = -\frac{1}{\pi}\frac{\mathrm{d}x(\lambda)}{\mathrm{d}\lambda} - \sum_{i,j=1,2}\int_{B_{ij}}^{\infty} \mathrm{d}\lambda' \; K(\lambda - \lambda')\sigma_{ij}(\lambda') \tag{A1}$$

The factor of 4 indicates 4 type of possible configurations and the constraint of exclusions in rapidities λ in solving the quantum inverse scattering problem. The idea is that in equilibrium four type of distributions are equally possible for each bound state bare energy $2x(\lambda)$. The B_{ij} play the role of chemical potentials for the Bethe-Ansatz momenta and are determined from the physical chemical potentials of the two leads, μ_i, by minimizing the charge free energy,

$$F = \sum_i (E_i - \mu_i N_i) = \sum_i \int_{B_{ij}}^{\infty} \mathrm{d}\lambda \; (x(\lambda) - \mu_i)\sigma_{(i)}(\lambda) d\lambda$$

with $\sigma_{(1)} \equiv 2\sigma_{11} + \sigma_{12} + \sigma_{21}$ the lead 1 particle density and $\sigma_{(2)} \equiv 2\sigma_{22} + \sigma_{12} + \sigma_{21}$ the lead 2 particle density. In the case of $\mu_1 > \mu_2$ we have $B_{11} < B_{12} = B_{21} < B_{22}$ for this finite U Anderson model but the equation for $\sigma_{ij}(\lambda)$ is the same for different combination of i and j. The reason is we put a quasi-hole state, rather than a quasi-particle, in the integral equation Eq.(A1) similar to the treatment of Wiener-Hopf approach. For example, for $B_{11} < \lambda < B_{22}$ there could be three type of quasi-particle state $\{ij\} = \{11, 12, 21\}$ and we put $\{ij\} = \{22\}$ state as quasi-hole state. This hole state still count one weight of the probability of 4 distributions and therefore the factor of 4 on the left hand side of Eq.(A1) retains even out of equilibrium. Similar idea is also applied in two type of bound state (strings) solution.

Other than their differences in the density distribution the computations for the current and dot occupation expectation value are quite similar to the two strings case. We show their numerical results in the following.

The differential conductance vs voltage as shown in Fig.14, obtained by taking numerical derivative on current vs voltage data, essentially gives the same picture as in two strings case, namely a sharp Kondo peak nearby $V = 0$ and a broad side peak corresponding to charge fluctuations. In the case of $\langle n_d \rangle$ vs V, however, there is an additional feature occurring at an energy scale higher than the energy scale of the charge fluctuation side peak (corresponding to the voltage position of 2nd peak shown in the inset) as shown in Fig. 15. This is especially apparent if we looked at the nonequilibrium charge susceptibility as shown in inset of Fig.15.

As we do not expect there should be any further charge fluctuations, we rule out, by physical argument, the possibility of 4 strings configuration.

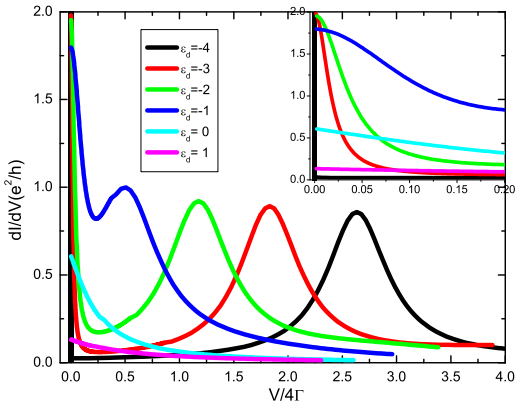

FIG. 14: $\frac{dI}{dV}$ vs $\frac{V}{4\Gamma}$ for $U = 8$, $\Gamma = 0.25$ and various ϵ_d from $\epsilon_d = -\frac{U}{2}$ to $\epsilon_d = 1$. The inset is the enlarged region nearby zero voltage.

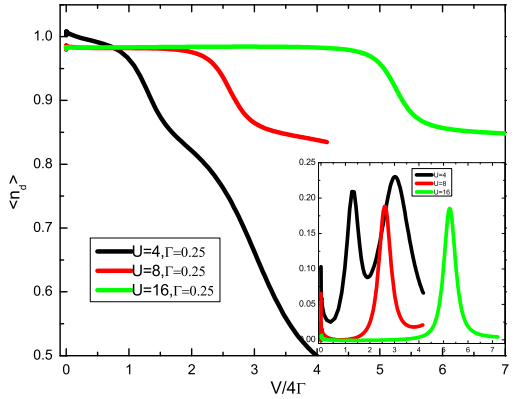

FIG. 15: $\langle n_d \rangle$ vs $\frac{V}{4\Gamma}$ for different U, $\Gamma = 0.25$ and $\epsilon_d = -\frac{U}{2}$. The inset is $-\frac{\partial \langle n_d \rangle}{\partial V}|_{\epsilon_d}$ vs V voltage. A third peak shows up in $U = 4$ case.

Appendix B: Two particles solution and choice of s_{op}

For the two particles solution we follow similar construction in P B Wiegmann and A M Tsvelick's work[31] and the Scattering Bethe Ansatz approach developed by P. Mehta and N. Andrei[7]. Since Eq.(1) is rotational invariant the spin quantum number is conserved. We show the solution with both particles with spin singlet incoming from lead 1 as an example in the following. Spin quantum number in z direction S_z is a good quantum number and we can write the two particle solution of $S_z = 0$ state as:

$$\begin{aligned}|\Psi\rangle = \Big\{ \int dx_1 dx_2 \{ & Ag(x_1,x_2)\psi^\dagger_{e\uparrow}(x_1)\psi^\dagger_{e\downarrow}(x_2) \\ +Ch(x_1,x_2)\psi^\dagger_{o\uparrow}(x_1)\psi^\dagger_{o\downarrow}(x_2) & + Bj(x_1,x_2)(\psi^\dagger_{e\uparrow}(x_1)\psi^\dagger_{o\downarrow}(x_2) \\ -\psi^\dagger_{e\downarrow}(x_1)\psi^\dagger_{o\uparrow}(x_2))\} & + \int dx (Ae(x)(\psi^\dagger_{e\uparrow}(x)d^\dagger_\downarrow - \psi^\dagger_{e\downarrow}(x)d^\dagger_\uparrow) \\ + Bo(x)(\psi^\dagger_{o\uparrow}(x)d^\dagger_\downarrow - \psi^\dagger_{o\downarrow}(x)d^\dagger_\uparrow)) & + Amd^\dagger_\uparrow d^\dagger_\downarrow \Big\}|0\rangle\end{aligned}$$

Here A, B, C are arbitrary constants to be determined later. To satisfy $\hat{H}|\Psi\rangle = E|\Psi\rangle = (k+p)|\Psi\rangle$ we have:

$$\begin{aligned}
0 &= [-i(\partial_{x_1}+\partial_{x_2}) - E]g(x_1,x_2) \\
&\quad +t[\delta(x_1)e(x_2) + \delta(x_2)e(x_1)] && \text{(B1)}\\
0 &= [-i(\partial_{x_1}+\partial_{x_2}) - E]h(x_1,x_2) && \text{(B2)}\\
0 &= [-i(\partial_{x_1}+\partial_{x_2}) - E]j(x_1,x_2) + t\delta(x_1)o(x_2) && \text{(B3)}\\
0 &= (-i\partial_x - E + \epsilon_d)e(x) + tg(0,x) + t\delta(x)m && \text{(B4)}\\
0 &= (-i\partial_x - E + \epsilon_d)o(x) + tj(0,x) && \text{(B5)}\\
0 &= (U+2\epsilon_d)m + 2te(0) - Em && \text{(B6)}
\end{aligned}$$

For $U = 0$ the model becomes non-interacting and the two particles solution becomes direct product of two one particle solutions.

$$\begin{aligned}|\Psi\rangle &= |\psi_{k\uparrow}\rangle \otimes |\psi_{p\downarrow}\rangle + |\psi_{p\uparrow}\rangle \otimes |\psi_{k\downarrow}\rangle \\ = \int dx_1 dx_2 \{ & (g_k(x_1)\psi^\dagger_{e\uparrow}(x_1) + h_k(x_1)\psi^\dagger_{o\uparrow}(x_1) + e_k d^\dagger_\uparrow \delta(x_1)) \\ & (g_p(x_2)\psi^\dagger_{e\downarrow}(x_2) + h_p(x_2)\psi^\dagger_{o\downarrow}(x_2) + e_p d^\dagger_\downarrow \delta(x_2)) \\ + & (g_p(x_1)\psi^\dagger_{e\uparrow}(x_1) + h_p(x_1)\psi^\dagger_{o\uparrow}(x_1) + e_p d^\dagger_\uparrow \delta(x_1)) \\ & (g_k(x_2)\psi^\dagger_{e\downarrow}(x_2) + h_k(x_2)\psi^\dagger_{o\downarrow}(x_2) + e_k d^\dagger_\downarrow \delta(x_2))\}|0\rangle\end{aligned}$$

Therefore at $U = 0$ we have:

$$\begin{aligned}
g(x_1,x_2) &= g_k(x_1)g_p(x_2) + g_k(x_2)g_p(x_1) \\
h(x_1,x_2) &= h_k(x_1)h_p(x_2) + h_k(x_2)h_p(x_1) \\
j(x_1,x_2) &= g_k(x_1)h_p(x_2) + h_k(x_2)g_p(x_1) \\
e(x) &= e_k g_p(x) + e_p g_k(x) \\
o(x) &= e_k h_p(x) + e_p h_k(x) \\
m &= 2e_p e_k
\end{aligned}$$

Now for $U \neq 0$ we shall derive the solution of this form

$$\begin{aligned}g(x_1,x_2) &= Z_{kp}(x_1-x_2)g_k(x_1)g_p(x_2) \\ &\quad + Z_{kp}(x_2-x_1)g_k(x_2)g_p(x_1) && \text{(B7)}\end{aligned}$$

Plug Eq.(B7) into Eq.(B1) we get

$$e(x) = Z_{kp}(-x)g_p(x)e_k + Z_{kp}(x)g_k(x)e_p \qquad \text{(B8)}$$

Plugging above two results into Eq.(B4) into Eq.(B6) we get for $m = 2\tilde{Z}_{kp}(0)e_k e_p$ we have:

$$\begin{aligned}
&(-i\partial_x Z_{kp}(-x))g_p(x)e_k + (-i\partial_x Z_{kp}(x))g_k(x)e_p \\
&-tZ_{kp}(-x)e_p\delta(x)e_k \\
&-tZ_{kp}(x)e_k\delta(x)e_p + 2tZ^*_{kp}(0)e_k e_p = 0 && \text{(B9)}\\
&2\tilde{Z}_{kp}(0)e_k e_p \\
&= \frac{2t(Z_{kp}(0)g_p(0)e_k + Z_{kp}(0)g_k(0)e_p)}{p+k-U-2\epsilon_d} && \text{(B10)}
\end{aligned}$$

Now take $Z_{kp}(x) = e^{-i\phi_{kp}}\theta(-x) + e^{i\phi_{kp}}\theta(x)$ we get $\tan(\phi_{kp}) = \frac{-Ut^2}{(k-p)(p+k-U-2\epsilon_d)}$ and $\tilde{Z}_{kp}(0) = \frac{k+p-2\epsilon_d}{k+p-U-2\epsilon_d}Z_{kp}(0)$. Define $\Gamma \equiv \frac{t^2}{2}$ and $B(k) \equiv k(k-2\epsilon_d-U)$ as in Ref. 32 we can rewrite $\tan(\phi_{kp}) = \frac{-2U\Gamma}{(B(k)-B(p))}$.

From Eq.(B2) we can write $h(x_1,x_2)$ as:

$$\begin{aligned}h(x_1,x_2) &= Z^{oo}_{kp}(x_1-x_2)h_k(x_1)h_p(x_2) \\ &\quad + Z^{oo}_{kp}(x_2-x_1)h_k(x_2)h_p(x_1) && \text{(B11)}\end{aligned}$$

with arbitrary $Z^{oo}_{kp}(x_1-x_2)$. Now write $j(x_1,x_2)$ as:

$$\begin{aligned}j(x_1,x_2) &= Z^{eo}_{kp}(x_1-x_2)g_k(x_1)h_p(x_2) \\ &\quad + Z^{eo}_{kp}(x_2-x_1)h_k(x_2)g_p(x_1) && \text{(B12)}\end{aligned}$$

again with $Z^{eo}_{kp}(x_1-x_2)$ undetermined. Plug Eq.(B12) into Eq.(B3) we get $o(x)$ is written as:

$$o(x) = Z^{eo}_{kp}(-x)h_p(x)e_k + Z^{eo}_{kp}(x)h_k(x)e_p \qquad \text{(B13)}$$

Now if we choose $Z^{eo}_{kp}(x_1-x_2) = Z_{kp}(x_1-x_2)$ and plug Eq.(B12) and Eq.(B13) into Eq.(B5) we get:

$$\begin{aligned}
&(-k+\epsilon_d)Z_{kp}(-x)h_p(x)e_k + (-p+\epsilon_d)Z_{kp}(x)h_k(x)e_p \\
&+t(Z_{kp}(-x)h_p(x)g_k(0) + Z_{kp}(x)h_k(x)g_p(0)) \\
&+(-i)(\partial_x Z_{kp}(-x))h_p(x)e_k + (-i)(\partial_x Z_{kp}(x))h_k(x)e_p \\
&= -2\sin(\phi_{kp})(h_p(0)e_k - h_k(0)e_p) = 0 && \text{(B14)}
\end{aligned}$$

To satisfy Eq.(B14) we can set $h_p(0) = 0$ for arbitrary p. This can be done by choosing $s_{op} = -4$ in Eq.(3). Now since $Z^{oo}_{kp}(x_1-x_2)$ is arbitrary we can choose $Z^{oo}_{kp}(x_1-x_2) = Z_{kp}(x_1-x_2)$. Also from Eq.(B10) we have

$$\tilde{Z}_{kp}(0) = \frac{p+k-2\epsilon_d}{p+k-U-2\epsilon_d}Z_{kp}(0) \qquad \text{(B15)}$$

Since the Hamiltonian in Eq.(1) has rotational invariance the general form of scattering matrix for particles with momentum k, p and spins σ_1, σ_2 is given by:

$$S^{\sigma_1'\sigma_2'}_{\sigma_1\sigma_2}(k,p) = b(k,p) + c(k,p)\hat{P}_{12} \qquad \text{(B16)}$$

where $\hat{P}_{12}=\frac{1}{2}(1\cdot 1+\vec{\sigma_1}\cdot\vec{\sigma_2})$ is the permutation operator in spins. For antiparallel spins (singlet state) as shown above $\hat{P}_{12}=-1$ thus we have:

$$\begin{aligned} b(k,p)-c(k,p) &= \frac{Z_{kp}(x>0)}{Z_{kp}(x<0)} \\ &= \frac{B(k)-B(p)-i2U\Gamma}{B(k)-B(p)+i2U\Gamma} \end{aligned} \quad \text{(B17)}$$

For the triplet state ($\hat{P}_{12}=1$) the interaction term with the impurity is absent and the particles passing through each other without changing their phase

$$b(k,p)+c(k,p)=1 \quad \text{(B18)}$$

Thus from Eq.(B17) and Eq.(B18) we get the two particle S-matrix as:

$$\hat{S}(k,p)=\frac{(B(k)-B(p))\mathbf{I}_{\tau,\tau'}+i2U\Gamma\mathbf{P}_{\tau,\tau'}}{B(k)-B(p)+i2U\Gamma} \quad \text{(B19)}$$

Thus the integrability of two lead with Anderson type dot system is the similar to the integrability of one lead Anderson model.

The choice of identical two particles S-matrices (by choosing $s_{op}=-4$) enables us to construct the scattering state labeled by lead indices by choosing appropriate A,B,C in this even-odd basis. For example, if both particles are coming from lead 1, we shall choose $(A,B,C)=A_0(\frac{t^2}{t_2^2},\frac{-t^2}{t_1t_2},\frac{t^2}{t_1^2})$ such that the amplitude of incoming state from lead 2 is zero (A_0 being an overall renormalization constant). We can therefore label the eigenstate by the incoming state from lead i and/or lead j. Without this s_{op} term we cannot write back from even-odd basis to lead indices basis in this two leads Anderson model and similarly in IRLM in Ref. 7.

Appendix C: Equivalence of TBA and SBA in equilibrium

Eq.(7) can be proved to be exact by comparing with the traditional Bethe Ansatz where $\langle\sum_\sigma d_\sigma^\dagger d_\sigma\rangle = 2\int_B^\infty \mathrm{d}\lambda\,\sigma_{\rm imp}(\lambda)$ with impurity density $\sigma_{\rm imp}(\lambda)$ given by

$$\sigma_{\rm imp}(\lambda)=\frac{\delta_{p^+}+\delta_{p^-}}{2\pi}-\int_B^\infty \mathrm{d}\lambda'\,K(\lambda-\lambda')\sigma_{\rm imp}(\lambda') \quad \text{(C1)}$$

By comparing Eq.(C1) and Eq.(5) in equilibrium ($\sigma_i(\lambda)=\sigma_b(\lambda)$ describing bulk quasi-particle density when $B_1=B_2=B$.) we get

$$\int_B^\infty \mathrm{d}\lambda\,\sigma_{\rm imp}(\lambda)\left(\frac{-1}{\pi}\frac{\mathrm{d}x(\lambda)}{\mathrm{d}\lambda}\right) = 2\int_B^\infty \mathrm{d}\lambda\,\sigma_b(\lambda)\left(\frac{\delta_{p^+}+\delta_{p^-}}{2\pi}\right) \quad \text{(C2)}$$

by noting that the integration kernel $K(\lambda-\lambda')$ is symmetric in λ and λ'. Since the equality is true for arbitrary B we can also rewrite Eq.(C2) as

$$\begin{aligned} \int_B^\infty \mathrm{d}\lambda\,\sigma_{\rm imp}(\lambda) &= 2\int_B^\infty \mathrm{d}\lambda\,\sigma_b(\lambda)\left(\frac{\delta_{p^+}+\delta_{p^-}}{-2\frac{\mathrm{d}x(\lambda)}{\mathrm{d}\lambda}}\right) \\ &\equiv 2\int_B^\infty \mathrm{d}\lambda\,\sigma_b(\lambda)\nu^{TBA}(\lambda) \end{aligned}$$

and the resulting $\nu^{TBA}(\lambda)$ is given by

$$\nu^{TBA}(\lambda)=\frac{-\tilde{x}(\lambda)\frac{y'(\lambda)}{x'(\lambda)}-\tilde{y}_-(\lambda)}{\tilde{x}^2(\lambda)+\tilde{y}_+^2(\lambda)} + \frac{\tilde{x}(\lambda)\frac{y'(\lambda)}{x'(\lambda)}+\tilde{y}_+(\lambda)}{\tilde{x}^2(\lambda)+\tilde{y}_+^2(\lambda)} \quad \text{(C3)}$$

Now let us show the computation for $\nu^{SBA}(\lambda)$. First we write one particle state of Eq.(1) in even channel (with $s_{ek}=0$ for the moment) as

$$\begin{aligned} |k,\sigma\rangle &= \int e^{ikx}\alpha^\dagger_{ek,\sigma}(x)dx|0\rangle \\ &= \int e^{ikx}\{(\bar{\theta}+A_k\theta)\psi^\dagger_{e\sigma}+B_k d^\dagger_\sigma\delta(x)\}dx|0\rangle \end{aligned} \quad \text{(C4)}$$

Solving $\hat{H}|k,\sigma\rangle=k|k,\sigma\rangle$ we get

$$\begin{aligned} -i(-1+A_k)+B_k t&=0 \\ \epsilon_d B_k+t\frac{1+A_k}{2}&=kB_k \end{aligned}$$

Thus we get $A_k=\frac{k-\epsilon_d-i\frac{t^2}{2}}{k-\epsilon_d+i\frac{t^2}{2}}$ and $B_k=\frac{t}{k-\epsilon_d+i\frac{t^2}{2}}$. We may also define $g_k(x)=e^{ipx}(\bar{\theta}+A_k\theta)$ and $e_k=B_k$ to have easier comparison with Wiegmann and Tsvelick's work[31]. The two particles state is obtained by constructing product of two $\alpha^\dagger_{ep,\sigma}(x)$ particles state with appropriate two particles S-matrix expressed in $Z_{k^+k^-}(x_1-x_2)$.

In principle we shall use $|\Psi,N_1,N_2\rangle$ as the many body state to compute expectation value. However the simplification here, similar to the case of IRLM in Ref.7, is that different λ (corresponding to different $p(\lambda)$) are orthogonal to each other in $L\to\infty$ limit. Thus the many body expectation value can be obtained via two body computation and the rest just get canceled by normalization factor. We shall demonstrate the explicit computation for two particles in the following.

Denote $|\Psi\rangle$ as the two particles solution. We may write spin singlet state as

$$
\begin{aligned}
|\Psi\rangle &= \int dx_1 dx_2 \mathcal{A}\left\{e^{i(kx_1+px_2)} Z_{kp}(x_1-x_2)\alpha^\dagger_{ek,\uparrow}(x_1)\alpha^\dagger_{ep,\downarrow}(x_2)\right\}|0\rangle \\
&= \int dx_1 dx_2 \Big\{ Z_{kp}(x_1-x_2)\{g_k(x_1)g_p(x_2)\psi^\dagger_\uparrow(x_1)\psi^\dagger_{e\downarrow}(x_2) + g_k(x_1)e_p\psi^\dagger_\uparrow(x_1)d^\dagger_\downarrow\delta(x_2) \\
&\quad + e_k g_p(x_2)d^\dagger_\uparrow\delta(x_1)\psi^\dagger_\downarrow(x_2) + e_k e_p d^\dagger_\uparrow d^\dagger_\downarrow\delta(x_1)\delta(x_2)\} - Z_{kp}(x_2-x_1)\{g_k(x_2)g_p(x_1)\psi^\dagger_{e\downarrow}(x_2)\psi^\dagger_{e\uparrow}(x_1) \\
&\quad + g_k(x_2)e_p\psi^\dagger_{e\downarrow}(x_2)d^\dagger_\uparrow\delta(x_1) + e_k g_p(x_1)d^\dagger_\downarrow\delta(x_2)\psi^\dagger_{e\uparrow}(x_1) + e_k e_p d^\dagger_\downarrow d^\dagger_\uparrow\delta(x_1)\delta(x_2)\}\Big\}|0\rangle \\
&= \Big\{ \int dx_1 dx_2 [Z_{kp}(x_1-x_2)g_k(x_1)g_p(x_2) + Z_{kp}(x_2-x_1)g_k(x_2)g_p(x_1)]\psi^\dagger_{e\uparrow}(x_1)\psi^\dagger_{e\downarrow}(x_2) \\
&\quad + \int dx [Z_{kp}(x)g_k(x)e_p + Z_{kp}(-x)g_p(x)e_k](\psi^\dagger_{e\uparrow}(x)d^\dagger_\downarrow - \psi^\dagger_{e\downarrow}(x)d^\dagger_\uparrow) + 2e_k e_p \tilde{Z}_{kp}(0)d^\dagger_\downarrow d^\dagger_\uparrow\Big\}|0\rangle
\end{aligned}
$$

With $\mathcal{A}$ denoting anti-symmetrization and $\tilde{Z}_{kp}(0) = \frac{k+p-2\epsilon_d}{k+p-U-2\epsilon_d} Z_{kp}(0)$.

Solving $\hat{H}|k,\sigma;p,-\sigma\rangle = (k+p)|k,\sigma;p,-\sigma\rangle$ we obtain

$$
Z_{kp}(x_1-x_2) = \theta(x_1-x_2) + \frac{(k-p)(k+p-2\epsilon_d-U)-iUt^2}{(k-p)(k+p-2\epsilon_d-U)+iUt^2}\theta(x_2-x_1)
$$

For the case of bound state the two particle S-matrix is given by $Z_{k^+k^-}(x_1-x_2) = \theta(x_1-x_2) \equiv \theta^x_{12}$. The normalization factor and matrix element of dot occupation given by the even channel two particles wavefunction are

$$
\begin{aligned}
\langle\Psi|\Psi\rangle &= \int dy_1 dy_2 \int dx_1 dx_2 (\theta^y_{12} g_{k^+}(y_1)g_{k^-}(y_2) + \theta^y_{21} g_{k^+}(y_2)g_{k^-}(y_1))^* \\
&\quad \times(\theta^x_{12} g_{k^+}(x_1)g_{k^-}(x_2) + \theta^x_{21} g_{k^+}(x_2)g_{k^-}(x_1))\delta(x_1-y_1)\delta(x_2-y_2) \\
&\quad +2\int dy \int dx [\theta(y)g_{k^+}(y)e_{k^-} + \theta(-y)g_{k^-}(y)e_{k^+}]^*[\theta(x)g_{k^+}(x)e_{k^-} + \theta(-x)g_{k^-}(x)e_{k^+}]\delta(x-y) \\
&\quad +4(e_{k^+}e_{k^-}\tilde{Z}_{k^+k^-}(0))^*(e_{k^+}e_{k^-}\tilde{Z}_{k^+k^-}(0)) \\
\sum_\sigma \langle\Psi|\hat{d}^\dagger_\sigma\hat{d}_\sigma|\Psi\rangle &= 2\int dy \int dx [\theta(y)g_{k^+}(y)e_{k^-} + \theta(-y)g_{k^-}(y)e_{k^+}]^*[\theta(x)g_{k^+}(x)e_{k^-} + \theta(-x)g_{k^-}(x)e_{k^+}]\delta(x-y) \\
&\quad +8(e_{k^+}e_{k^-}\tilde{Z}_{k^+k^-}(0))^*(e_{k^+}e_{k^-}\tilde{Z}_{k^+k^-}(0)) \\
&= 2\left\{\int dx[\theta(x)|g_{k^+}(x)e_{k^-}|^2 + \theta(-x)|g_{k^-}(x)e_{k^+}|^2] + 4|e_{k^+}e_{k^-}\tilde{Z}_{k^+k^-}(0)|^2\right\}
\end{aligned}
$$

Note that the even channel bound state can be written as sum over bound state of $\{11,12,21,22\}$ (4 strings type) or $\{11,22\}$ (2 strings type) with the same real part of energy $k = x(\lambda)$. This can be viewed as the consistency counting from Fock basis to Bethe basis as electrons in lead 1 and lead 2 has 4 fold degeneracies in its initial state (2 different spins in each lead). Also note that

$$\begin{aligned}
\int dx_1 dx_2\ \theta_{12}^x |g_{k^+}(x_1) g_{k^-}(x_2)|^2 &= \int dx_1 dx_2 |e^{i(k^+ x_1 + k^- x_2)}(\bar{\theta}_1 + \theta_1 A_{k^+})(\bar{\theta}_2 + \theta_2 A_{k^-})|^2 \theta_{12} \\
&= \int dx_1 dx_2\ e^{-2\xi_k (x_1 - x_2)} |\bar{\theta}_1 \bar{\theta}_2 \theta_{12} + \theta_1 \bar{\theta}_2 \theta_{12} A_{k^+} + \theta_1 \theta_2 \theta_{12} A_{k^+} A_{k^-}|^2 \\
&= \left(\frac{L}{2\xi_k} - \frac{1 - e^{-2\xi_k L}}{(2\xi_k)^2} \right) \left(1 + |A_{k^+} A_{k^-}|^2\right) + \left(\frac{1 - e^{-2\xi_k L}}{2\xi_k} \right)^2 |A_{k^+}|^2 \\
\int dx\, \theta(x) |g_{k^+}(x) e_{k^-}|^2 &= \int dx\, \theta(x) |e^{i(k + i\xi_k)x} (\theta(-x) + A_{k^+} \theta(x)) e_{k^-}|^2 = \int_0^L dx\, e^{-2\xi_k x} |A_{k^+} e_{k^-}|^2 \\
&= \frac{1}{2\xi_k} \left| \frac{k - \epsilon_d + i\xi_k - i\Gamma}{k - \epsilon_d + i\xi_k + i\Gamma} \frac{t}{k - \epsilon_d - i\xi_k + i\Gamma} \right|^2 = \frac{1}{2\xi_k} \left| \frac{t}{k - \epsilon_d + i\xi_k + i\Gamma} \right|^2 \\
\int dx\, \theta(-x) |g_{k^-}(x) e_{k^+}|^2 &= \int dx\, \theta(-x) |e^{i(k - i\xi_k)x} (\theta(-x) + A_{k^-} \theta(x)) e_{k^+}|^2 = \int_{-L}^0 dx\, e^{2\xi_k x} |A_{k^-} e_{k^+}|^2 \\
&= \frac{1}{2\xi_k} \left| \frac{t}{k - \epsilon_d + i\xi_k + i\Gamma} \right|^2
\end{aligned}$$

with $\tilde{Z}_{k^+k^-}(0) = \frac{2(k-\epsilon_d)}{2(k-\epsilon_d)-U} Z_{k^+k^-}(0)$ and $Z_{k^+k^-}(0) = \frac{1}{2}$ based on our regularization scheme. By expressing $k = x(\lambda)$ and $\xi_k = y(\lambda)$ and taking $L \to \infty$ thus preserving $\frac{1}{L}$ terms only we get

$$\begin{aligned}
\frac{\langle \Psi | \sum_\sigma \hat{d}_\sigma^\dagger \hat{d}_\sigma | \Psi \rangle}{\langle \Psi | \Psi \rangle} &= \frac{1}{L} \nu^{SBA}(\lambda) \qquad \text{(C5)} \\
&= \frac{1}{L} \left\{ \frac{2\Gamma}{\tilde{x}^2(\lambda) + \tilde{y}_+^2(\lambda)} + \frac{16 y(\lambda) \Gamma^2}{(\tilde{x}^2(\lambda) + \tilde{y}_-^2(\lambda))(\tilde{x}^2(\lambda) + \tilde{y}_+^2(\lambda))} \left(\frac{\tilde{x}(\lambda)}{2\tilde{x}(\lambda) - U} \right)^2 \right\} .
\end{aligned}$$

By expressing $\nu^{TBA}(\lambda)$ and $\nu^{SBA}(\lambda)$ in λ explicitly we see that $\nu^{TBA}(\lambda) = \nu^{SBA}(\lambda)$. Since $\langle \sum_\sigma d_\sigma^\dagger d_\sigma \rangle = 2 \int_B^\infty d\lambda \sigma_{imp}(\lambda)$ in TBA we have proved that the expectation value evaluated by the state we constructed is exact and the equivalence of SBA and TBA in equilibrium in this two-lead Anderson model.

[1] D. Goldhaber-Gordon, H. Strickman, D. Mahalu, D. Abusch-Magder, U. Meirav and M. A. Kastner, Nature **391**, 156 (1998) M. Grobis, I. G. Rau, R. M. Potok, H. Shtrikman, and D. Goldhaber-Gordon, Phys. Rev. Lett. **100**, 246601 (2008)

[2] J. Schmid, J. Weis, K. Eberl, and K. Von Klitzing, Physica **B258**, 182 (1998)

[3] S. M. Cronenwett, T. H. Oosterkamp and L. P. Kouwenhoven, Science **281**, 540 (1998)

[4] S. M. Cronenwett, H. J. Lynch, D. Goldhaber-Gordon, L. P. Kouwenhoven, C. M. Marcus, K. Hirose, N. S. Wingreen, and V. Umansky, Phys. Rev. Lett. **88**, 226805 (2002)

[5] W. G. van der Wiel, S. De Franceschi, T. Fujisawa, J. M. Elzerman, S. Tarucha, L. P. Kouwenhoven, Science **289** 2105 (2000)

[6] J. Park, A. N. Pasupathy, J. I. Goldsmith, C. Chang, Y. Yaish, J. R. Petta, M. Rinkoski, J. P. Sethna, H. D. Abruna, P. L. McEuen, and D. C. Ralph, Nature **417**, 722 (2002)

[7] P. Mehta and N. Andrei, Phys. Rev. Lett. **96**, 216802 (2006) ibid. **100**, 086804 (2008). See also cond-mat/0702612 for more detailed discussion of techniques of Scattering Bethe Ansatz and cond-mat/0703426.

[8] T. K. Ng and P. A. Lee, Phys. Rev. Lett. **61**, 1768 (1988)

[9] Glazman, L. I. and Raikh, M. E., JETP Letters,**47**, 452 (1988)

[10] Y. Meir and N. Wingreen, Phys. Rev. **B 49**, 11040 (1994)

[11] M. Pustilnik and L. I. Glazman, Phys. Rev. Lett. **87**, 216601 (2001)

[12] M H. Hettler and H. Schoeller, Phys. Rev. Lett. **74**, 4907 (1995)

[13] A. Oguri, Phys. Rev. **B 64**, 153305 (2001)
[14] A. Oguri, J. Phys. Soc. Jpn. **74**, 110 (2005)
[15] Z. Ratiani and A. Mitra, Phys. Rev. **B 79**, 245111 (2009)
[16] A. Rosch, J. Kroha, and P. Wölfle, Phys. Rev. Lett. **87**, 156802 (2001)
[17] J. Eckel, F. Heidrich-Meisner, S. G. Jakobs, M. Thorwart, M. Pletyukhov and R. Egger, cond-mat/1001.3773 (2010)
[18] F. Heidrich-Meisner, A. E. Feiguin, and E. Dagotto, Phys. Rev. **B 79**, 235336 (2009)
[19] R. V. Roermund, S-Y Shiau and M. Lavagna, cond-mat/1001.3873 (2010)
[20] D. Matsumoto, J. Phys. Soc. Jpn. **69** , 1449 (2000)
[21] C. D. Spataru, M. S. Hybertsen, S. G. Louie, and A. J. Millis , Phys. Rev. **B 79**, 155110 (2009)
[22] A. Schiller and N. Andrei, cond-mat/0710.0249 (2007).
[23] E. Boulat and H. Saleur, Phys. Rev. **B 77**, 033409 (2008)
[24] E. Boulat, H. Saleur and P. Schmitteckert, Phys. Rev. Lett. **101**, 140601 (2008)
[25] J. S. Langer and V. Ambegaokar, Phys. Rev. **121**, 1090 (1961)
[26] D. C. Langreth, Phys. Rev. **150**, 516 (1966)
[27] R. M. Konik, H. Saleur, and A. Ludwig, Phys. Rev. Lett. **87**, 236801 (2001)
[28] R. M. Konik, H. Saleur, and A. Ludwig, Phys. Rev. **B 66**, 125304 (2002)
[29] P. Fendley, A.W.W. Ludwig, H. Saleur, Phys. Rev. **B 52**, 8934 (1995)
[30] P. Fendley, A.W.W. Ludwig, H. Saleur, Phys. Rev. Lett. **74**, 3005 (1995)
[31] P. B. Wiegman and A. M. Tsvelik, J. Phys. **C. 16**, 2281 (1983); P. B. Wiegman and A. M. Tsvelik, Adv. in Phys. **32**, 453 (1983)
[32] N. Kawakami and A. Okiji, J. Phys. Soc. Jap. 51, 1145 (1982); N. Kawakami and A. Okiji, Solid State Commun. 43, 365 (1982)
[33] The thermodynamic Bethe Ansatz proof of ground state configuration for two leads case was done by C. J. Bolech and then by S. P. Chao, unpublished.
[34] A renormalizable Hamiltonian such as the Anderson model requires regularization and a cut-off scheme to define it. The results are universal once the cut-off is removed. In intermediate stages as the cut off is finite it is important to adopt a scheme that does not break integrability. The scheme adopted here satisfies this requirement. N.Andrei, K. Furuya and J. H. Lowenstein, Rev. Mod. Phys. **56**, 331 (1984), section VI. In our regularization scheme the locally discontinuous function $s(x) \equiv \theta(x)\theta(-x)$ satisfies $\partial_x s(x) = 0$.
[35] Without the regularization factor in the odd sector the model is still integrable. However, it is not possible to identify the fixed number of incoming particles by this choice, A. Nishino and N. Hatano in J. Phys. Soc. Jpn. **76**, 063002 (2007).
[36] N. Kawakami and A. Okiji, Phys. Rev. **B 42**, 2383 (1990)
[37] D. K.K. Lee and P. A. Lee, Physica **B 259-261** , 481 (1999)
[38] This dressed energy is the sum of the dressed energy of spinon and that of antiholon nearby equilibrium Fermi surface.
[39] N. Andrei, Phys. Lett. **A 87**, 299 (1982).
[40] A. O. Gogolin, R.M. Konik, A.W.W. Ludwig, and H. Saleur, Ann. Phys. (Leipzig) **16**, No. 10?1, 678 (2007).
[41] The equality can be proved analytically in linear response. In numerics we also see very good agreement, especially for large voltage, with voltage computed by $\mu_1 - \mu_2$ given by free energy and voltage computed by difference in particle number.
[42] F. D. M. Haldane, Phys. Rev. Lett. **40**, 416 (1978)
[43] A.C. Hewson, A. Oguri, and D. Meyer, Eur. Phys. J. **B 40**, 177 (2004)
[44] J. Paaske and K. Flensberg, Phys. Rev. Lett. **94**, 176801 (2005)
[45] A. C. Hewson, *The Kondo Problem to Heavy Fermions*, Cambridge Studies in Magnetism (1993).
[46] Here we adopted the Kondo scale as in the article by N. S. Wingreen and Y. Meir, Phys. Rev. **B 49**, 11040 (1994). We put a factor of $\sqrt{10}$ to increase this scale so the Kondo peak can be observed more easily in numerics.
[47] E. Lebanon and A. Schiller, Phys. Rev. **B 65**, 035308 (2001)